

A night-side shock aurora and its three different emissions observed on 26 February 2023

Sota Nanjo¹, Masatoshi Yamauchi², Magnar Gullikstad Johnsen³, Yoshihiro Yokoyama², Urban Brändström⁴, and Keisuke Hosokawa¹

¹University of Electro-Communications

²Swedish Institute of Space Physics

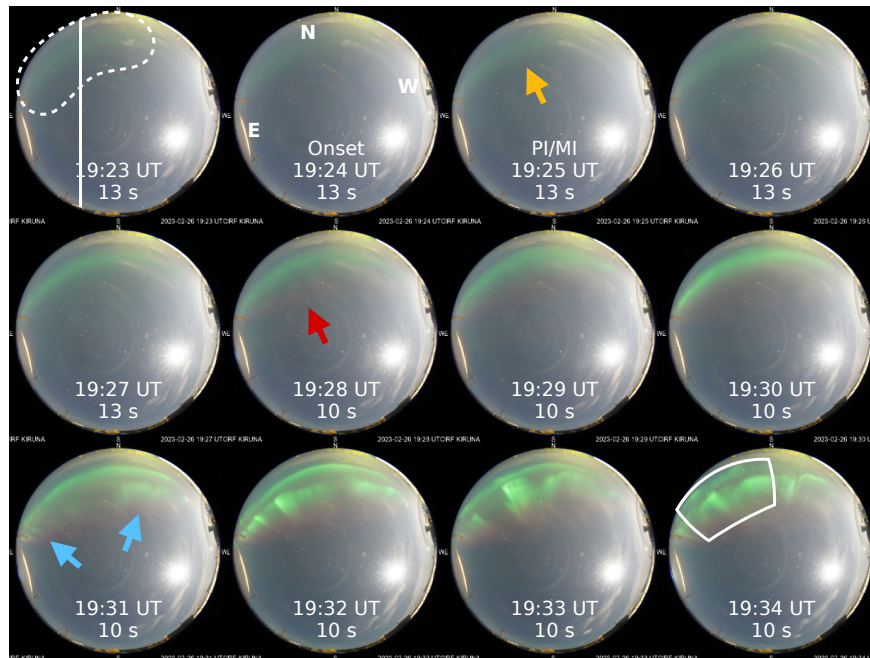
³UiT the Arctic University of Norway

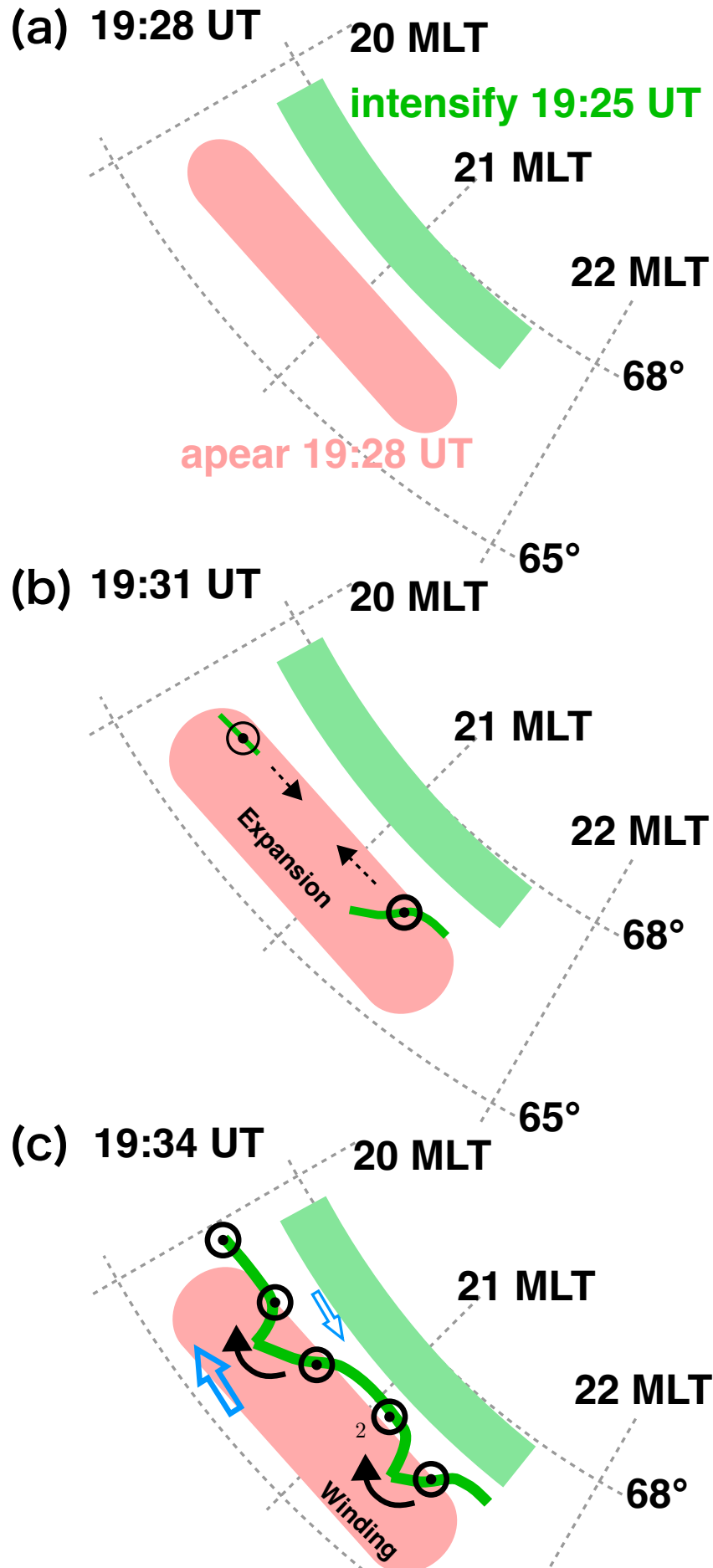
⁴Institute of Space Physics

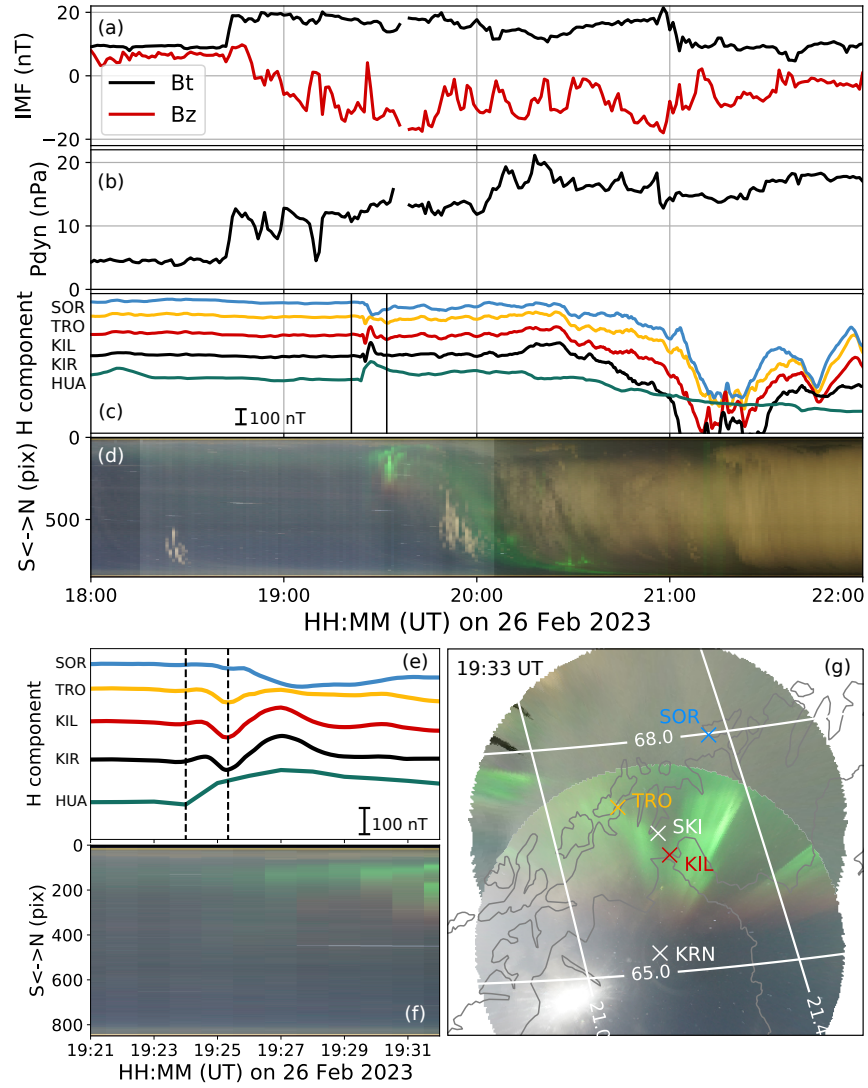
March 26, 2023

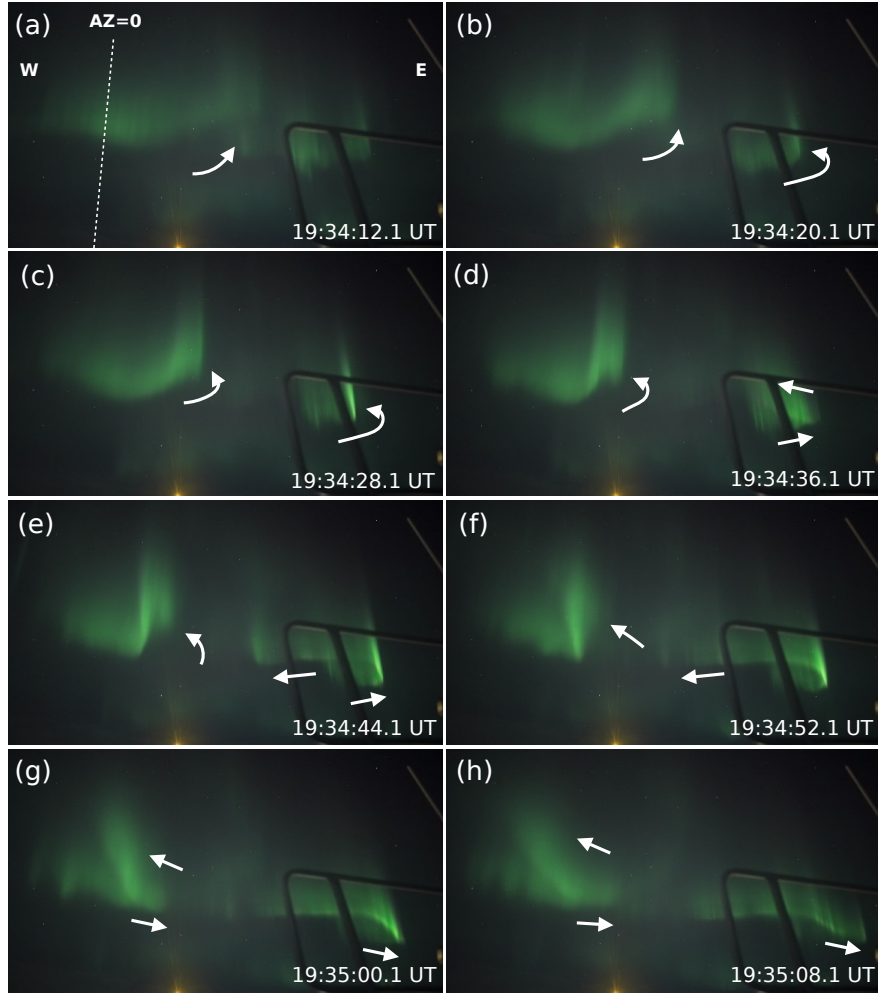
Abstract

Ground-based observations of shock aurora, which is an aurora related to geomagnetic sudden commencement (SC), have mainly been limited to the dayside. On 26 February 2023, right after the SC onset at 19:24 UT, ground-based all-sky cameras and a wide-angle camera detected shock aurora at 21 MLT in the auroral zone. For this aurora, three different emissions are detected instead of the previously known two emissions: intensification of a pre-existing arc (19:25 UT), red diffuse aurora (19:28 UT), and a second, green discrete arc (19:31 UT). The relative location of these emissions differs from the dayside cases where the first and last types are not distinguished. Geomagnetic data under this aurora indicates a significant difference in the anti-sunward propagation velocity between the secondary discrete arc and the related field-aligned current.









Hosted file

959320_0_supp_10826387_rryv21.docx available at <https://authorea.com/users/598040/articles/631600-a-night-side-shock-aurora-and-its-three-different-emissions-observed-on-26-february-2023>

A night-side shock aurora and its three different emissions observed on 26 February 2023

Nanjo, S.¹, M. Yamauchi², M. G. Johnsen³, Y. Yokoyama², U. Brändström²,
and K. Hosokawa¹

¹Graduate School of Communication Engineering and Informatics, The University of

Electro-Communications, Tokyo, Japan

²Swedish Institute of Space Physics (IRF), Kiruna, Sweden

³Tromsø Geophysical Observatory, Tromsø, Norway

Key Points:

- Three types of shock aurora, instead of two, are observed at 21 MLT by ground-based cameras.
- They most likely correspond to three different geomagnetic signatures of an SC: DL, PI, and MI.
- The propagation speeds of the current and aurora can be different for the MI signature.

Corresponding author: Sota Nanjo, sota.nanjo@uec.ac.jp

Abstract

Ground-based observations of shock aurora, which is an aurora related to geomagnetic sudden commencement (SC), have mainly been limited to the dayside. On 26 February 2023, right after the SC onset at 19:24 UT, ground-based all-sky cameras and a wide-angle camera detected shock aurora at 21 MLT in the auroral zone. For this aurora, three different emissions are detected instead of the previously known two emissions: intensification of a pre-existing arc (19:25 UT), red diffuse aurora (19:28 UT), and a second, green discrete arc (19:31 UT). The relative location of these emissions differs from the dayside cases where the first and last types are not distinguished. Geomagnetic data under this aurora indicates a significant difference in the anti-sunward propagation velocity between the secondary discrete arc and the related field-aligned current.

Plain Language Summary

Ground-based observations of “shock aurora” related to “sudden commencement (SC),” which is a sudden geomagnetic activity caused by a rapid increase of the solar wind speed (such as caused by a solar storm), were previously limited to the dayside. However, the recent development of dense networks of auroral cameras and magnetometers allows us to examine the shock aurora in the nightside from the ground. On 26 February 2023, shortly after the onset of an SC at 19:24 UT, ground-based all-sky cameras and a wide-angle camera detected the shock aurora at 21 MLT in the auroral zone. Three distinct optical emissions, instead of the two emissions previously observed on the dayside, appeared with clear time delay and locational difference: intensification of a pre-existing arc (19:25 UT), red diffuse aurora (19:28 UT), and a secondary green discrete aurora (19:31 UT). There are also other differences from dayside observations: the last emission had a different propagation speed than the related field-aligned current, and the relative location of the three emissions was different.

1 Introduction

Geomagnetic sudden commencement (SC), which is caused by a rapid increase in solar wind dynamic pressure, consists of a stepwise increase and subsequent bipolar spike in the geomagnetic field (Araki, 1994, and references therein). These Disturbances are the most outstanding ground magnetic field perturbation at Low latitudes and the Polar region, hence called DL and DP, respectively. DP is normally divided into two parts, the preliminary pulse, PI, and the main pulse, MI. Following the model of Araki (1994), PI is associated with a field-aligned current (FAC) pair flowing into the afternoon auroral zone and out of the morning auroral zone while traveling anti-sunward. PI is replaced by the MI some minutes later which is a stationary FAC pair of opposite directions compared to the PI pair.

Both disturbances are ultimately caused by an intensification of the magnetopause current, of which the information propagates globally across the geomagnetic field as the compression (this causes the DL on the ground) and as the Alfvén mode that carries FACs along the geomagnetic field, creating dusk-to-dawn and dawn-to-dusk ionospheric electric field and relevant current system (this causes the DP on the ground). Hence, the DL appears almost simultaneously (less than tens of seconds) at all magnetic local time (MLT) regions. DP (actually the PI part) also appears nearly simultaneously at all latitudes, although it is related to a current system that takes time to develop. This is because the related electric field in the ionosphere can propagate almost instantaneously as a waveguide mode (Kikuchi, 2014).

64 Measuring the time delay from dayside to nightside is difficult because the be-
 65 ginning signature of MI is hidden by the DL (and even PI). Even the peak timing
 66 is not well determined because the duration and peak timing of the MI in the polar
 67 cap (anti-sunward convection side) depends on latitudes (Araki & Allen, 1982). One
 68 method for estimating the propagation velocity of the MI is to measure the optical
 69 aurora, which is typically colocated with the intensification of FACs. The optical au-
 70 rora related to an SC is actually observed by ground-based all-sky cameras (ASCs)
 71 and ultraviolet (UV) imagers onboard satellites (Kozlovsky et al., 2005; Liu et al.,
 72 2011), and is called shock aurora. Motoba et al. (2009) examined a shock aurora at
 73 15 MLT and identified both the PI-related diffuse patch (558 nm: green) equator-
 74 ward of a pre-existing arc and the MI-related discrete arc (558 nm and 630 nm: red)
 75 poleward the PI-related diffuse aurora. The relative location of the MI-related arc
 76 and pre-existing arc changes with the interplanetary magnetic field (IMF) and may
 77 overlap with each other (seen as an enhanced oval) for the northward IMF (Nishimura
 78 et al., 2016).

79 Nishimura et al. (2016) also obtained the spatial distribution of FACs and their
 80 temporal development using the magnetometer network in the northern hemisphere
 81 and compared it with images from ASC in Antarctica. The result suggests that the
 82 PI and MI correspond to diffuse and discrete auroras in the afternoon sector, respec-
 83 tively. Since the optical signature of the aurora provides a finer FAC structure than
 84 what a network of geomagnetic field measurements can provide, observation by cam-
 85 eras is necessary to reveal the detail of the SC current system. The method should
 86 have been applied to the nightside, but the only report from the ground-based opti-
 87 cal measurements is by meridian scanning photometers (Holmes et al., 2014). With-
 88 out such optical observations, we do not know how the FAC develops as it propa-
 89 gates to the nightside or even whether the aurora types are the same between day-
 90 side and nightside.

91 According to the global imaging from satellites, the MI(PI)-related electron au-
 92 rora propagates anti-sunward at about 4–6 km/s (10 km/s) on the duskside (dawn-
 93 side) ionosphere (Zhou & Tsurutani, 1999; Holmes et al., 2014), and the shock au-
 94 rora can extend to the midnight sector. Using multiple scanning photometers, which
 95 are separately installed by about 1100 km in the evening sector and 900 km in the
 96 morning sector, Holmes et al. (2014) demonstrated that the anti-sunward propa-
 97 gation speed is consistent with the result from satellite observations. The derived
 98 speed in the evening sector corresponds to 1–1.5 MLT/min, requiring 8 min from
 99 dayside to nightside (20–22 MLT), consistent with the start of the MI signature 6
 100 min after the SC onset. On the other hand, Holmes et al. (2014) detected the red
 101 (630 nm) emission 1 minute before the appearance of the green (558 nm) aurora,
 102 which indicates that low-energy electrons may have precipitated into the ionosphere
 103 3 min prior to the high-energy (> 1 keV) electrons if we take into account the av-
 104 erage relaxation time of the red aurora of about 2 min. The FAC corresponding to
 105 the duskside red aurora must have arrived much earlier than the source FAC for the
 106 green aurora in Holmes et al. (2014), giving a quite different anti-sunward propaga-
 107 tion speed between the source of the red aurora and that of the green aurora.

108 To summarize our understanding so far, there are two types of shock aurora in
 109 addition to pre-existing arc: the PI-related and MI-related auroras, and they might
 110 have different propagation speeds from each other. If so, the difference in the ap-
 111 pearance time of these auroras would be larger on the nightside than on the day-
 112 side. In addition, the relative location of these auroras and even the fine structure
 113 might also be different between dayside and nightside. To clearly distinguish these
 114 auroras and their temporal development on the nightside, we need observations of
 115 multi-wavelength cameras and a dense meridional network of the magnetometer in
 116 the auroral region.

117 On 26 February 2023, right after an SC onset at 19:24 UT, a color ASC in
 118 Kiruna that was located at 21 MLT (65° geomagnetic latitude) detected (1) the en-
 119 hancement of a pre-existing green arc (19:25 UT), (2) the appearance of a red diffuse
 120 aurora (19:28 UT), and (3) a secondary green arc (19:31 UT) at unexpected location
 121 (equatorward of the pre-existing arc), with the geomagnetic MI peak at 19:27 UT.
 122 We also observed the secondary arc with a high-time resolution wide-angle camera,
 123 which revealed the vortex motion of the arc. The shock aurora was weakened within
 124 20 min, and this interval was isolated from the subsequent substorm growth phase.
 125 The shock aurora appeared above the densely distributed magnetometer network
 126 (IMAGE), and the relative location of FACs and aurora can be derived in good reso-
 127 lution. Here we report these combined observations of the shock aurora seen 3 hours
 128 before the magnetic midnight.

129 2 Instruments

130 2.1 All-sky cameras (ASCs)

131 We analyzed all-sky images from cameras in Kiruna, Sweden (67.83°N , 20.42°E)
 132 and Skibotn, Norway (69.35°N , 20.36°E). In Kiruna, a Sony $\alpha 7\text{S}$ with a Nikkor 8mm
 133 F2.8 lens was installed. The camera's ISO was set at 4000, and the exposure time
 134 was 10–13 sec. Images were taken every minute. At Skibotn Observatory, a Sony
 135 $\alpha 6400$ with a MEIKE MK-6.5mm F2.0 lens was in operation. The camera's ISO was
 136 set at 8000, and the exposure time was 8 sec. Images were taken every 30 sec. We
 137 used these images to geolocate and identify spatiotemporal variations of the aurora.

138 2.2 Wide-angle camera (WAC)

139 A Sony $\alpha 7\text{SIII}$ with an FE 24mm F1.4 GM lens was installed at a dome where
 140 the Kiruna ASC was located. This camera, called wide-angle camera (WAC), faces
 141 in the north-northeast direction at a low elevation with an angle of view of ~ 73 de-
 142 grees horizontally, covering an area marked by a white rectangle in the last panel of
 143 Figure 2. WAC recorded videos at 30 frames per second, offering a high temporal
 144 resolution for visualizing auroral movement within 1 minute. WAC has 1920×1080
 145 pixels, an ISO sensitivity of 80000, and a 1/30 second exposure time. We averaged
 146 15 images (for 0.5 seconds) to make snapshots to reduce noise, as shown in Figure 3.
 147 We provide a video of the event as Supporting Information.

148 2.3 Magnetometers

149 A selection of magnetometers from the IMAGE network has been applied in
 150 the study. These are stable flux-gate magnetometers, providing 10-second resolution
 151 data. Furthermore, the low latitude, Intermagnet magnetometer at Huancayo has
 152 been used.

153 3 Observation Results

154 Figures 1a and 1b shows the IMF (intensity in black and the z component in
 155 red) and solar wind dynamic pressure, respectively, from the Deep Space Climate
 156 Observatory (DSCOVR). A stepwise enhancement of the IMF intensity and dynamic
 157 pressure, a typical signature of the interplanetary shock, was detected at around
 158 18:40 UT. Figure 1c shows the H component of the geomagnetic field recorded by
 159 magnetometers located in Sørøya (SOR), Norway (70.54°N , 22.22°E); Tromsø (TRO),
 160 Norway (69.66°N , 18.94°E); Kilpisjärvi (KIL), Finland (69.02°N , 20.79°E); Kiruna
 161 (KIR), Sweden (67.83°N , 20.42°E); and Huancayo (HUA), Peru (12.06°S , 75.21°W).
 162 Their locations, except HUA, are shown in Figure 1g. HUA is instead located on the

163 dayside equator at ~ 14.2 MLT, which is the typical SC onset region. All the sta-
 164 tions show the SC signature starting at around 19:24 UT. This SC is isolated from
 165 the substorm activity that started around 20:20 UT, and hence we show only the
 166 short time interval in Figure 1e (19:21–19:32 UT). The onset time ($\sim 19:24:00$ UT)
 167 is marked by a dashed line (left). Similarly, the peak time of the PI ($\sim 19:25:20$ UT)
 168 is also marked by another dashed line (right).

169 Figures 1d and 1f show the keogram, the time series of the north-south cross-
 170 section of the all-sky images from Kiruna ASC. Note that the exposure time changed
 171 from 10 to 13 sec at 19:28 UT. The keogram shows that the aurora appeared shortly
 172 (~ 15 min) after the SC, and its intensity gradually increased for the first ~ 10 min.
 173 Figure 1f shows a time lag between the magnetic signatures and the auroral intensi-
 174 fication.

175 In Figure 1g, all-sky images obtained by the ASCs in Kiruna and Skibotn at
 176 19:33 UT are projected on the map showing the locations of the magnetic stations
 177 and cameras. Coordinates with an elevation angle of more than 20 degrees were
 178 used for the projection, and the auroral emission layer was assumed to be 100 km.
 179 The projected aurora is found close to the zenith of Kilpisjärvi and Tromsø (67.5°
 180 MLAT, 21 MLT).

181 Figure 2 is a minute-by-minute all-sky image from 19:23 to 19:34 UT. The up-
 182 per side of each image is north, and the left side is east. The solid white line in the
 183 first panel shows the cross-section used to make keograms shown in Figure 1. The
 184 first all-sky image at 19:23 UT, taken before the SC onset, already shows a weak
 185 diffuse aurora (circled by the white dashed line) in the northeast direction. In this
 186 paper, we refer to this aurora as the pre-existing arc. The third all-sky image was
 187 taken 1 minute after the onset and shows that the arc is stronger than before the on-
 188 set, as indicated by the yellow arrow. At 19:28 UT, as indicated by the red arrow,
 189 a red emission became visible south of the pre-existing arc that was further intensi-
 190 fied. This intensification causes the automatic change in the exposure time from 13
 191 to 10 sec. At 19:31 UT, discrete arcs with wavy structures were detected between
 192 the pre-existing arc and the red emission at both the west (right) and east (left)
 193 sides. They were connected at 19:32 UT and formed an arc from west to east, and
 194 the wavy structure became stronger afterward. In this paper, we refer to this arc
 195 as the secondary arc. The last four all-sky images (19:31–19:34 UT) show the quick
 196 evolution of the secondary arc every minute. The 1-min resolution is apparently too
 197 low to visualize the exact fine spatiotemporal evolution of the secondary arc. For-
 198 tunately, we have a 30 Hz video taken by WAC. WAC captured the white rectangle
 199 region in the last all-sky image in Figure 2.

200 Figure 3 shows the images taken by WAC observing the area shown in the last
 201 panel of Figure 2. The images obtained from 19:34.12.1 to 19:35:08.1 UT are shown
 202 every 8 seconds. In the electronic version of this paper, a real-time video of this se-
 203 quence is provided as Supporting Information. Note that the east-west direction of
 204 the image is reversed from the all-sky image. The meridian with an azimuth angle of
 205 0 degrees (northward) is shown as a dotted line in panel (a). In each snapshot, two
 206 auroral structures are visible with a spatial gap near the center of the image. Both
 207 wavy structures gradually steepened by the westward motion on the front side (low
 208 latitude side) and eastward motion on the back side (high latitude side), as indicated
 209 by the white arrows. As this steepening developed, these structures consequently
 210 formed a spiral shape.

4 Discussion

The shock aurora was observed by ASCs and the high-speed WAC in the evening sector at around 21 MLT. Three components of shock aurora were identified instead of only two (PI-related diffuse aurora and MI-related arc), which was the case for the dayside afternoon sector. Their characteristics are summarized in Figure 4, in which the locations of the aurora are illustrated in the polar view.

1. Pre-existing weak arc (green, most likely 558 nm) was gradually intensified right after the SC onset at 19:24 UT.
2. Red diffuse aurora (apparently 630 nm) gradually appeared widely in the longitudinal direction equatorward of the intensified pre-existing arc, as shown in Figure 4a. This aurora became visible at 19:28 UT, i.e., 4 min after the onset.
3. Discrete green (secondary) arcs suddenly appeared between the red diffuse aurora and the intensified pre-existing arc at two separated spots (west and east in the WAC images). They became visible at 19:31 UT (7 min after the SC onset) and developed before start moving.

We also examined a video from the EMCCD ASC in Tjautjas, Sweden (attached as Supplemental Information), and found that the western and eastern arcs seen at 19:31 UT in Figure 2 appeared at around 19:30:52 and 19:31:12 UT, respectively. Both arcs did not propagate gradually but appeared as jump as independent clumps. The jumping speed from west to east (about 0.5 MLT apart) is about 1.5 MLT/min. After the appearance, both arcs started expanding in the east-west direction (Figure 4b) and got connected to each other. Subsequently, they showed the vortex motion without changing their locations, as shown in Figure 4c. The secondary arc might be accompanied by the red emission (most likely 630 nm) at high latitudes, but it is difficult to examine the continuity from the ASC images.

Considering the average relaxation time of ~ 2 min for the red diffuse aurora, the precipitation of the low-energy electrons might have started only 1–2 min after the SC onset. In the evening sector, diffuse auroras are generally associated with downward FAC, whereas intensified arcs are generally associated with upward FAC (e.g., Marklund et al., 2011). Therefore, the pre-existing arc (upward FAC) and red diffuse aurora (downward FAC) may be related to the DL and PI, respectively. In other words, the DL might also have generated the shock aurora by intensifying the pre-existing arc for the present case. If so, the past dayside observation of the MI-related aurora might be contaminated by the DL-related aurora.

The time delay of the appearance of the secondary arc from the SC onset was 7 min (and 5–6 min from the MI onset); thus, the anti-sunward propagation speed from the noon sector is about 1.5 MLT/min. This value is similar to the propagation/expansion speed of the MI-related arc in the afternoon sector (Motoba et al., 2009; Holmes et al., 2014; Nishimura et al., 2016). The nightside propagation speed estimated by the jumping of the secondary arc was also similar, about 1.5 MLT/min. Such an agreement indicates that the propagation of the MI-related aurora may be in the form of a leap rather than a continuous extension.

The secondary arc was located equatorward of the intensified pre-existing arc and overlapped with the red diffuse aurora, indicating that the source electric field existed at an L-shell in the middle of the ring current region. This implies that the affected areas in the nightside magnetosphere by the DL, PI, and MI are not in the same latitudinal order as the dayside signature in terms of the L-shell. This is not impossible if we consider the difference in the propagation velocities of the DL (compression) and DP (Alfvénic). If the relative latitude of the aurora is reversed between dayside and nightside, we must interpret the result from the meridian scan-

261 ning photometer (e.g., Holmes et al., 2014) in a different manner between dayside
 262 and nightside.

263 The present result also provides new insight into the anti-sunward propaga-
 264 tion speed of the FAC structure. Since the approximate FAC intensity is calculated
 265 from the latitudinal gradients of the H component of the geomagnetic field from
 266 the ground, the peak of FAC intensity read from Figure 1e (SOR, TRO, KIL, and
 267 KIR) is at 19:27 UT, i.e., 3 min after the SC onset at 19:24 UT. If we consider the
 268 start time of this gradient, the FAC already intensified at 19:26 UT, only 2 min after
 269 the SC onset. This means that the FAC propagated from dayside to 21 MLT with
 270 a speed of at least 4 MLT/min. This is much faster than the propagation speed of
 271 the MI-related aurora (1.5 MLT/min). Then the question is why the time delay be-
 272 tween the FAC and aurora intensification increases as it propagates anti-sunward.
 273 This question remains for future investigation.

274 Figures 3 and 4c show that the auroral vortex develops nearly stationary, sug-
 275 gesting that the anti-sunward convection poleward of the arc and sunward convec-
 276 tion equatorward of the arc have similar speeds. Such stationarity raises a ques-
 277 tion on the convection: how does the convection develop as the SC signature and
 278 shock aurora propagate anti-sunward? Together with the leap-like appearance, the
 279 formation of the aurora and its relation to the current system needs future investi-
 280 gations. Fortunately, modern optical instruments are rapidly improving their sen-
 281 sitivity, and the number of optical stations is increasing. Furthermore, the incom-
 282 ing SMILE (Solar wind Magnetosphere Ionosphere Link Explorer) mission to be
 283 launched in 2024–2025 would give a long-time global UV monitor from almost the
 284 same location. Combining its image with improved ground-based optical ability will
 285 allow systematic studies of the shock aurora on the nightside.

286 5 Conclusion

287 We observed the nightside shock aurora with ground-based all-sky cameras and
 288 a high-speed wide-angle camera at 21 MLT. Unlike the dayside shock aurora, where
 289 only two types of (PI- and MI-related) emissions are reported, we identified three
 290 emissions: enhancement of the pre-existing arc, the red diffuse aurora, and the dis-
 291 crete arc. These emissions most likely correspond to three different geomagnetic sig-
 292 natures of an SC: DL, PI, and MI. We believe that this is the first time observation
 293 of DL-related emission. For the MI signature, the anti-sunward propagation speed of
 294 the field-aligned current seems to be much faster than that of the related aurora. In
 295 addition, the relative location of the MI-related aurora and intensified pre-existing
 296 arc is not necessarily the same between the dayside and nightside.

Open Research Section

The all-sky images from Kiruna are available at <https://www.irf.se/alis/allsky/krn/2023/02/26/19/>. The all-sky images from Skibotn are available at http://darndeb08.cei.uec.ac.jp/~nanjo/public/skibotn_imgs/2022_season/20230226/. The solar wind data from DSCOVR are available at <https://www.ngdc.noaa.gov/dscovr/portal/index.html#/>. The magnetometer data from Huancayo is provided through INTERMAGNET <https://www.intermagnet.org>. Other magnetometer data are available at <https://flux.phys.uit.no/stackplot/>.

Acknowledgments

We thank Huancayo Geomagnetic Observatory and Finnish Meteorological Institute that provided the magnetometer data from Huancayo and Kilpisjärvi, respectively. We thank T. Araki for his valuable advice on SC. This work was partly supported by Grants-in-Aid for Scientific Research (15H05747, 22H00173, 21J20254) from the Japan Society for the Promotion of Science (JSPS). The first author of this study is a research fellow DC of JSPS.

References

- Araki, T. (1994). A physical model of the geomagnetic sudden commencement. In *Solar wind sources of magnetospheric ultra - low - frequency waves* (p. 183-200). American Geophysical Union (AGU). Retrieved from <https://agupubs.onlinelibrary.wiley.com/doi/abs/10.1029/GM081p0183> doi: <https://doi.org/10.1029/GM081p0183>
- Araki, T., & Allen, J. H. (1982). Latitudinal reversal of polarization of the geomagnetic sudden commencement. *Journal of Geophysical Research: Space Physics*, *87*(A7), 5207-5216. Retrieved from <https://agupubs.onlinelibrary.wiley.com/doi/abs/10.1029/JA087iA07p05207> doi: <https://doi.org/10.1029/JA087iA07p05207>
- Holmes, J. M., Johnsen, M. G., Deehr, C. S., Zhou, X.-Y., & Lorentzen, D. A. (2014). Circumpolar ground-based optical measurements of proton and electron shock aurora. *Journal of Geophysical Research: Space Physics*, *119*(5), 3895-3914. Retrieved from <https://agupubs.onlinelibrary.wiley.com/doi/abs/10.1002/2013JA019574> doi: <https://doi.org/10.1002/2013JA019574>
- Kikuchi, T. (2014). Transmission line model for the near-instantaneous transmission of the ionospheric electric field and currents to the equator. *Journal of Geophysical Research: Space Physics*, *119*(2), 1131-1156. Retrieved from <https://agupubs.onlinelibrary.wiley.com/doi/abs/10.1002/2013JA019515> doi: <https://doi.org/10.1002/2013JA019515>
- Kozlovsky, A., Safargaleev, V., Østgaard, N., Turunen, T., Koustov, A., Jussila, J., & Roldugin, A. (2005). On the motion of dayside auroras caused by a solar wind pressure pulse. *Annales Geophysicae*, *23*(2), 509-521. Retrieved from <https://angeo.copernicus.org/articles/23/509/2005/> doi: 10.5194/angeo-23-509-2005
- Liu, J. J., Hu, H. Q., Han, D. S., Araki, T., Hu, Z. J., Zhang, Q. H., ... Ebihara, Y. (2011). Decrease of auroral intensity associated with reversal of plasma convection in response to an interplanetary shock as observed over zhongshan station in antarctica. *Journal of Geophysical Research: Space Physics*, *116*(A3). Retrieved from <https://agupubs.onlinelibrary.wiley.com/doi/abs/10.1029/2010JA016156> doi: <https://doi.org/10.1029/2010JA016156>
- Marklund, G. T., Sadeghi, S., Cumnock, J. A., Karlsson, T., Lindqvist, P.-A., Nilsson, H., ... Zhang, Y. (2011). Evolution in space and time of the quasi-static acceleration potential of inverted-v aurora and its interaction with alfvénic

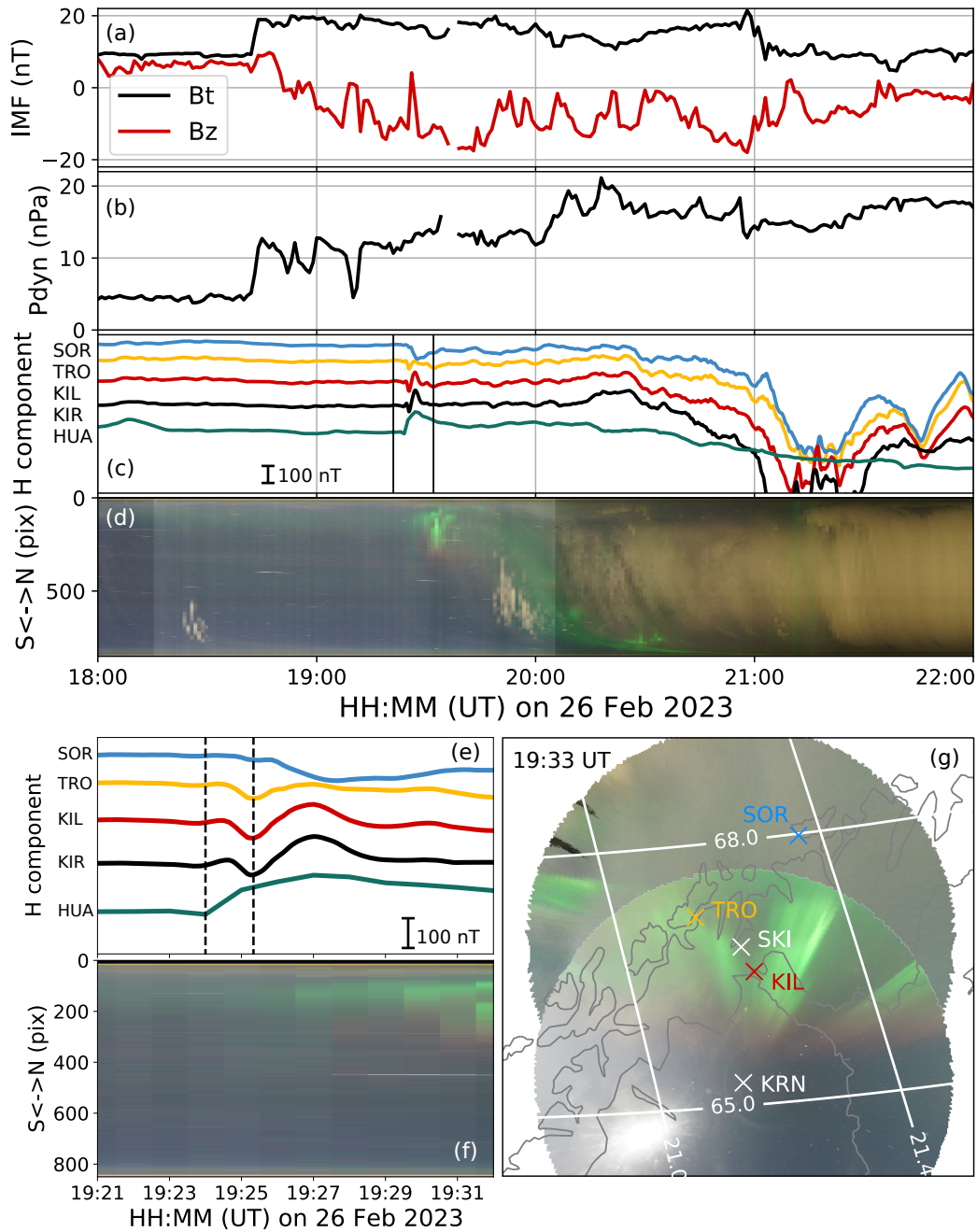


Figure 1. (a–b) The intensity (black) and z component (red) of the interplanetary magnetic field and solar wind dynamic pressure from DSCOVR. (c) Magnetometer data from the stations in the auroral and equatorial regions. A scale of 100 nT is shown in the lower left. (d) North-to-south keogram from the Kiruna ASC. (e–f) Close-up views of panels (c) and (d) from 19:21 to 19:32 UT. Vertical dashed lines indicate the onset of the SC and peak time of the PI. (g) Projection of all-sky images from the Kiruna and Skibotn ASCs. The location of the magnetometers is also shown. The grid line gives the magnetic local time and latitude.

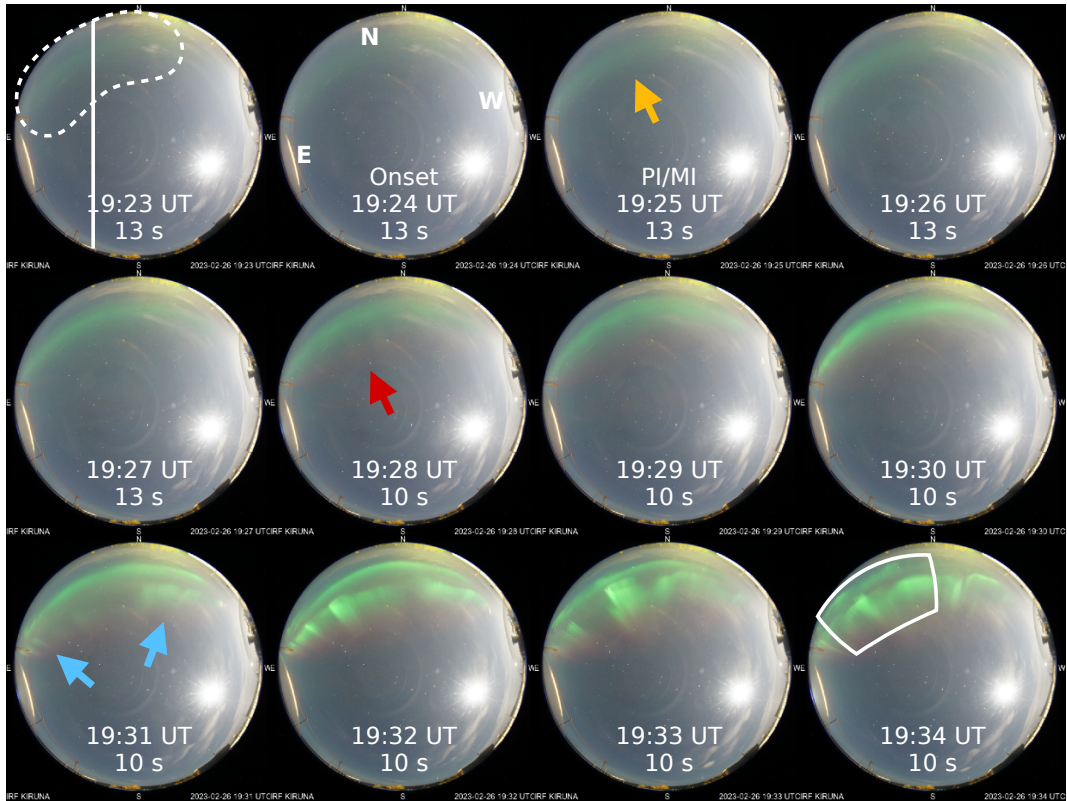


Figure 2. The ASC images from Kiruna during 19:23–19:34 UT on 26 February 2023. The top is north, and the left is east. The white dashed region in the first panel shows the pre-existing arc. The appearance of the red aurora and secondary arc is marked by red and blue arrows, respectively. The white rectangle region in the last panel is the FoV of the images shown in Figure 3.

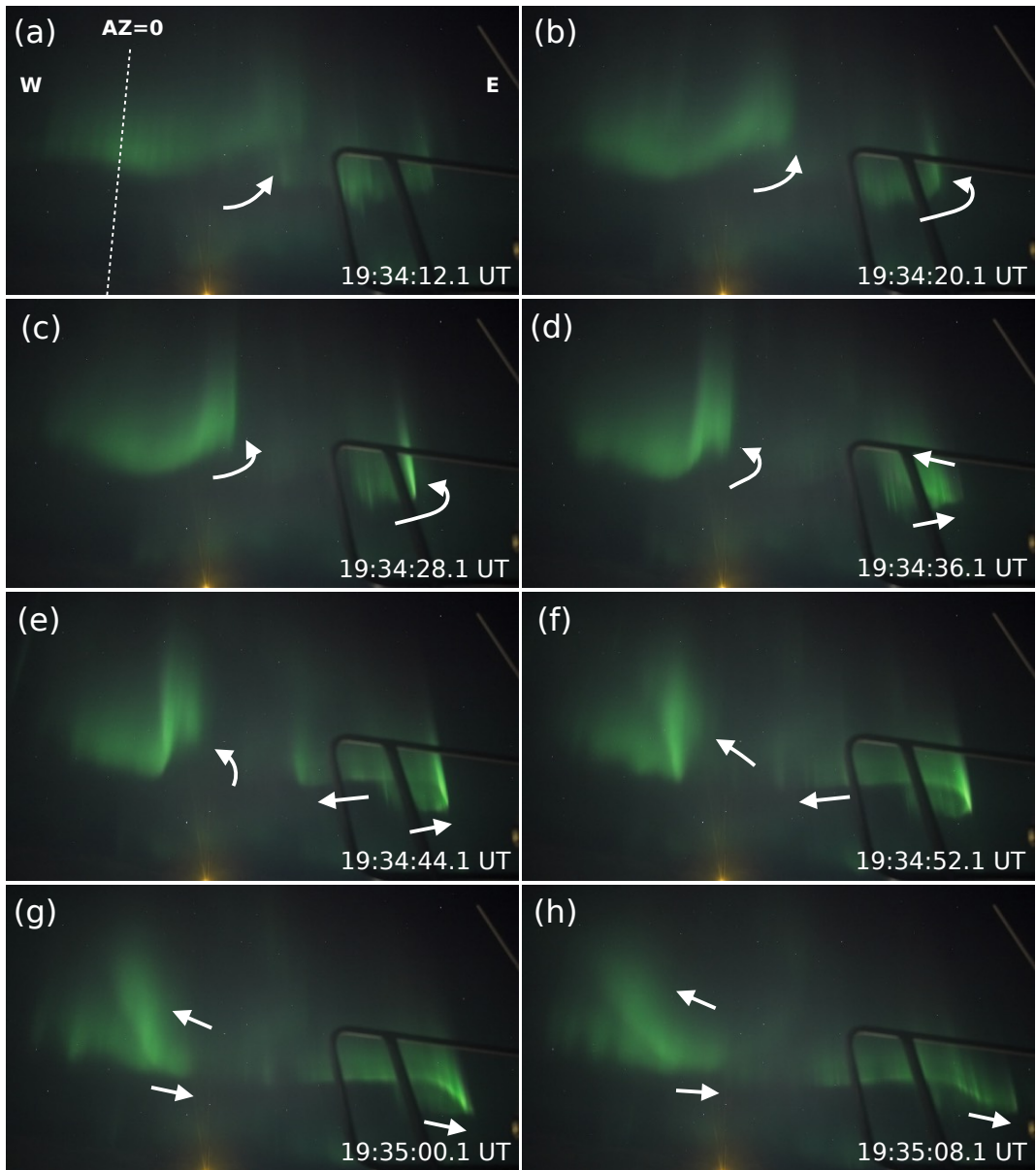


Figure 3. The wide-angle images captured by the Sony α 7SIII camera during 19:34:12–19:35:08 UT. The right side is east (different from the ASC image). The white dashed line in the first panel indicates the meridian, which has an azimuth angle of 0 degrees (towards the north). The white arrows guide the vortex motion.

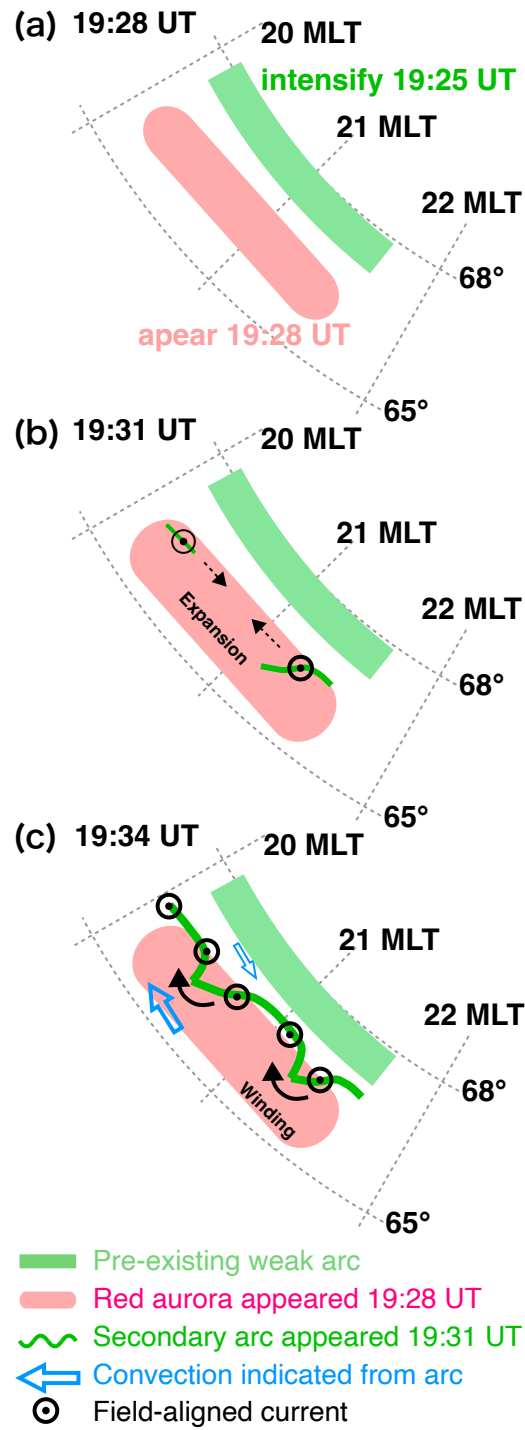


Figure 4. Schematic illustration of the relative locations of pre-existing arc, red diffuse aurora, and secondary arc. The blue arrows indicate the convection directions suggested by the vortex motion of the secondary arc.

- 348 boundary processes. *Journal of Geophysical Research: Space Physics*, 116(A1).
349 Retrieved from [https://agupubs.onlinelibrary.wiley.com/doi/abs/](https://agupubs.onlinelibrary.wiley.com/doi/abs/10.1029/2011JA016537)
350 [10.1029/2011JA016537](https://doi.org/10.1029/2011JA016537) doi: <https://doi.org/10.1029/2011JA016537>
- 351 Motoba, T., Kadokura, A., Ebihara, Y., Frey, H. U., Weatherwax, A. T., & Sato,
352 N. (2009). Simultaneous ground-satellite optical observations of postnoon
353 shock aurora in the southern hemisphere. *Journal of Geophysical Research:*
354 *Space Physics*, 114(A7). Retrieved from [https://agupubs.onlinelibrary](https://agupubs.onlinelibrary.wiley.com/doi/abs/10.1029/2008JA014007)
355 [.wiley.com/doi/abs/10.1029/2008JA014007](https://doi.org/10.1029/2008JA014007) doi: [https://doi.org/10.1029/](https://doi.org/10.1029/2008JA014007)
356 [2008JA014007](https://doi.org/10.1029/2008JA014007)
- 357 Nishimura, Y., Kikuchi, T., Ebihara, Y., Yoshikawa, A., Imajo, S., Li, W., & Utada,
358 H. (2016, Aug 11). Evolution of the current system during solar wind pressure
359 pulses based on aurora and magnetometer observations. *Earth, Planets and*
360 *Space*, 68(1), 144. Retrieved from [https://doi.org/10.1186/s40623-016](https://doi.org/10.1186/s40623-016-0517-y)
361 [-0517-y](https://doi.org/10.1186/s40623-016-0517-y) doi: [10.1186/s40623-016-0517-y](https://doi.org/10.1186/s40623-016-0517-y)
- 362 Zhou, X., & Tsurutani, B. T. (1999). Rapid intensification and propagation of
363 the dayside aurora: Large scale interplanetary pressure pulses (fast shocks).
364 *Geophysical Research Letters*, 26(8), 1097-1100. Retrieved from [https://](https://agupubs.onlinelibrary.wiley.com/doi/abs/10.1029/1999GL900173)
365 [agupubs.onlinelibrary.wiley.com/doi/abs/10.1029/1999GL900173](https://doi.org/10.1029/1999GL900173) doi:
366 <https://doi.org/10.1029/1999GL900173>

Figure 1.

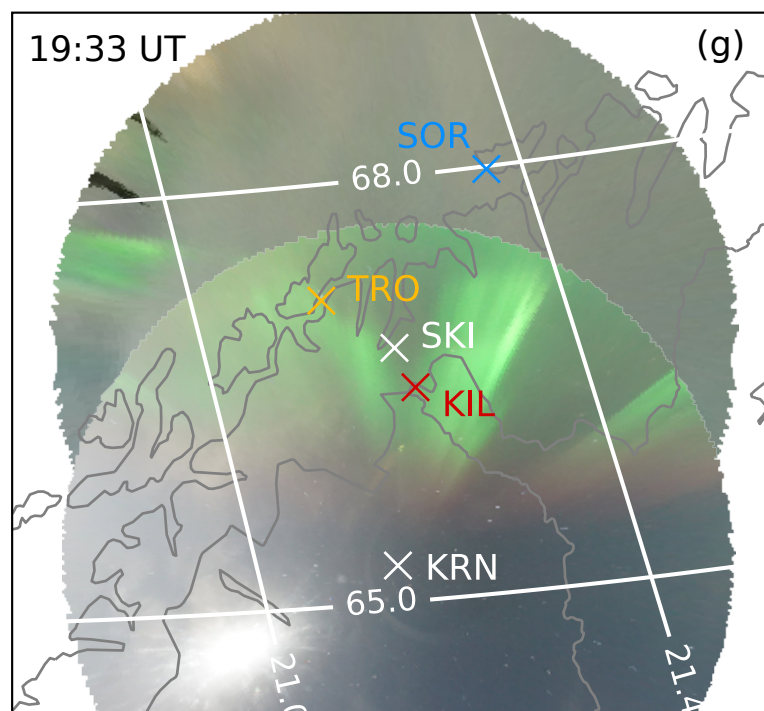
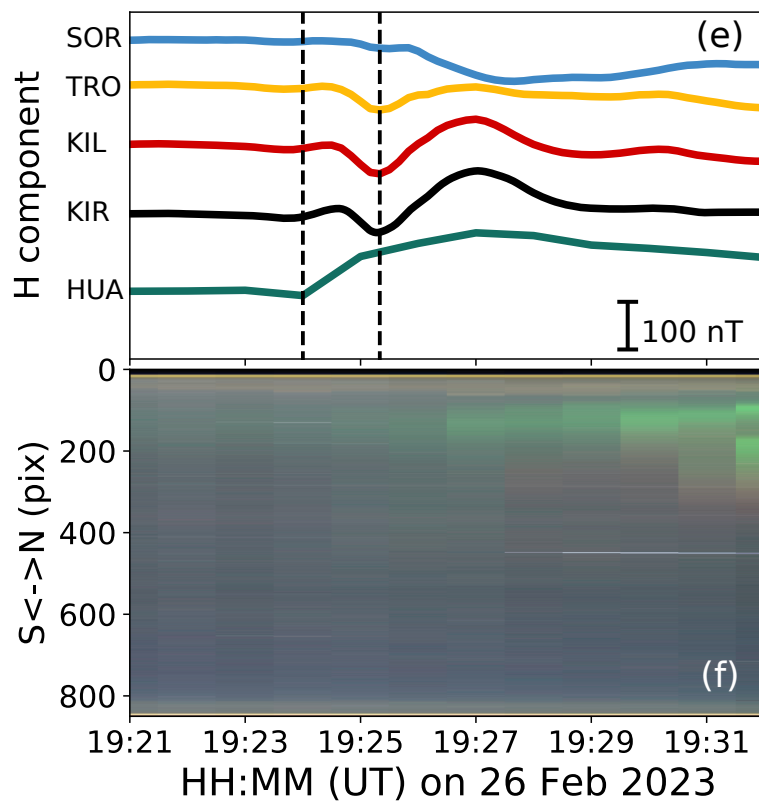
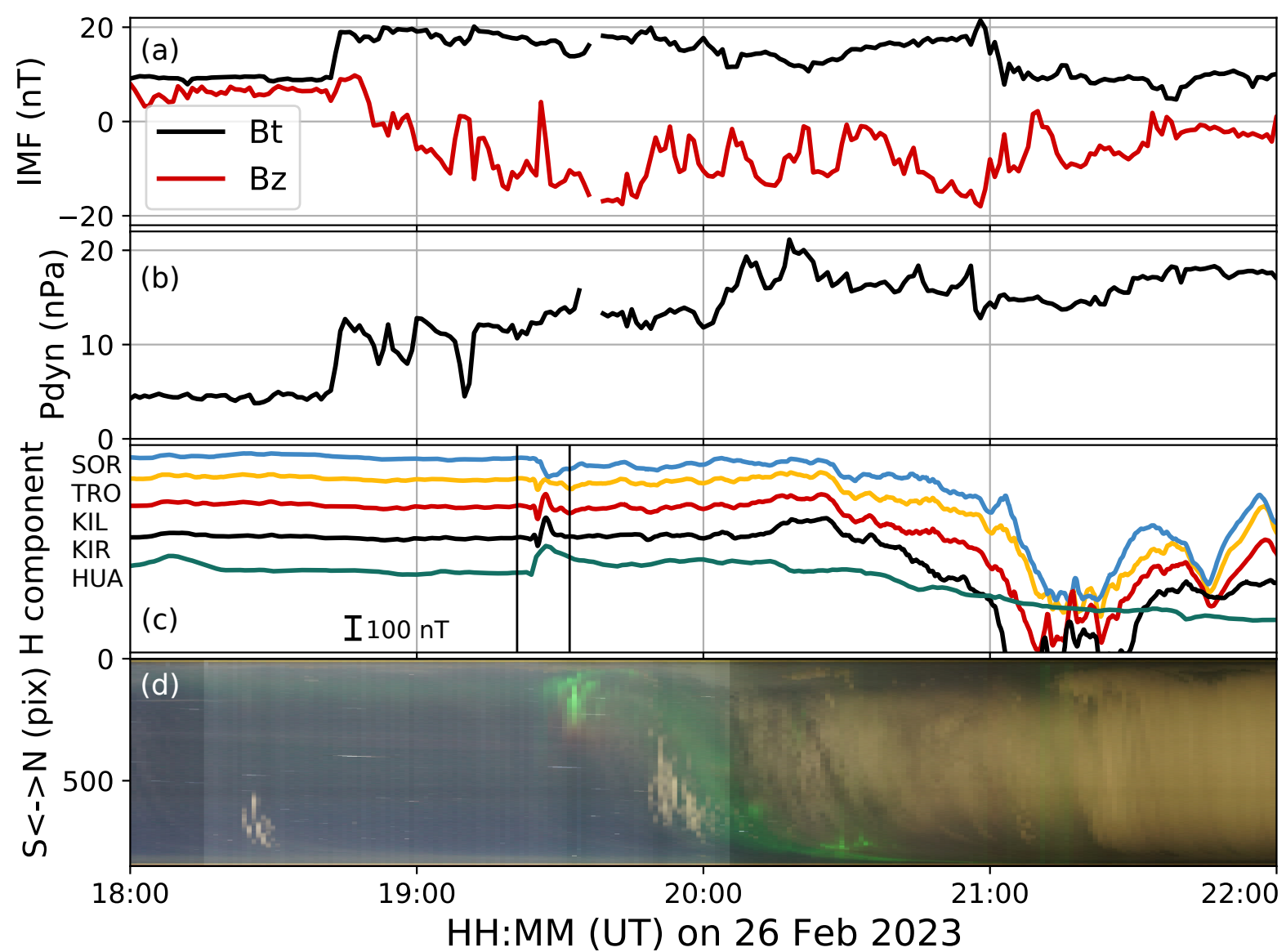


Figure 2.

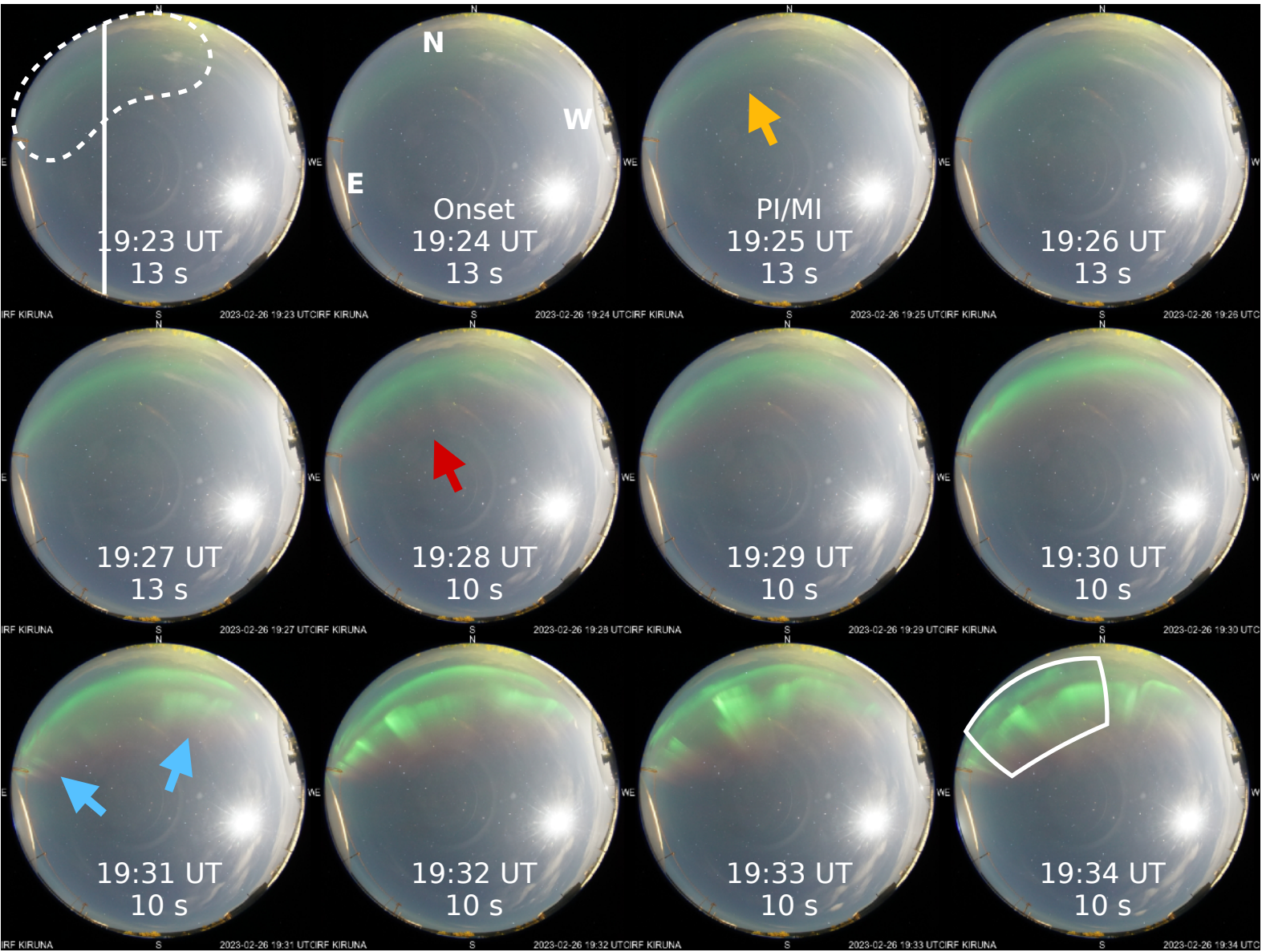


Figure 3.

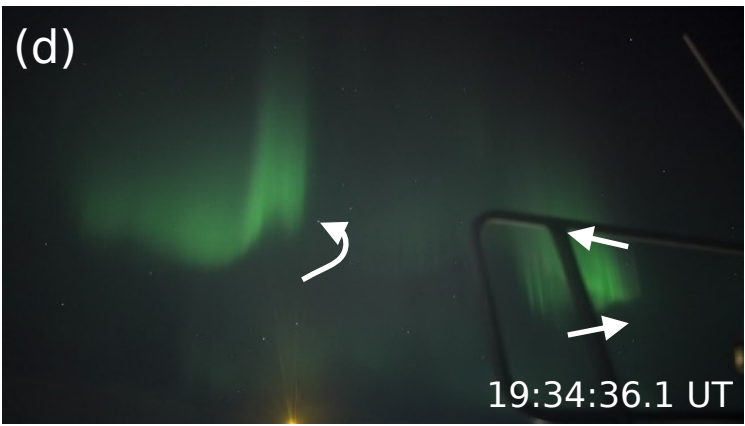
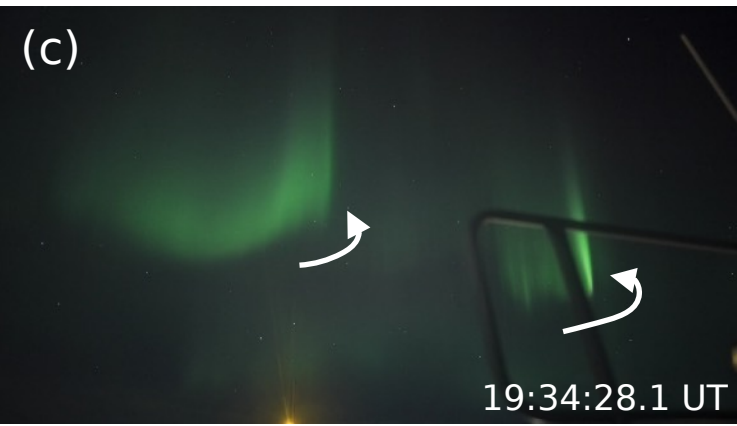
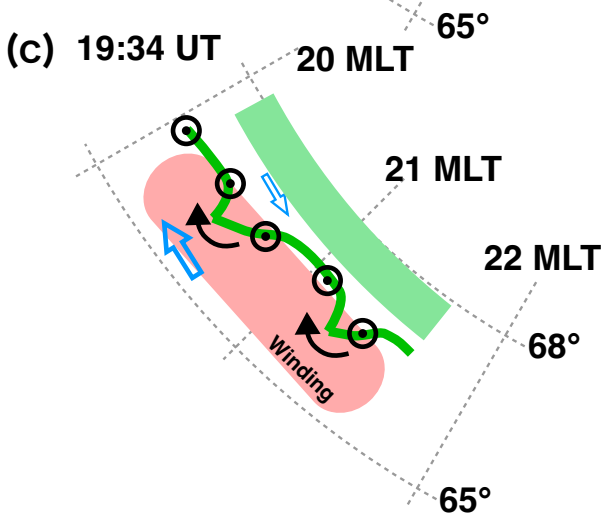
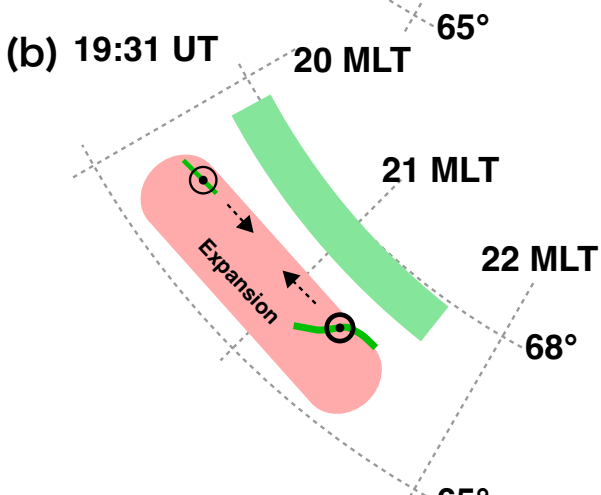
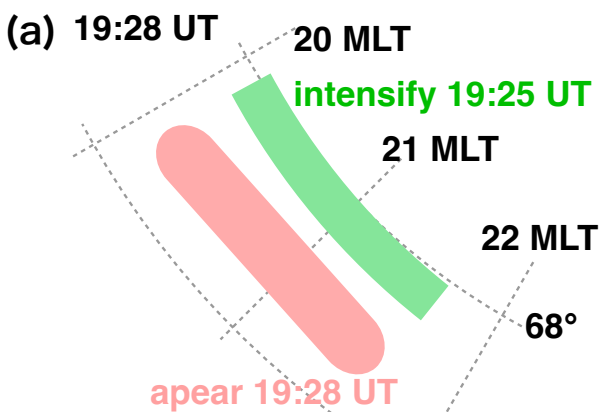


Figure 4.



- █ Pre-existing weak arc
- █ Red aurora appeared 19:28 UT
- ~ Secondary arc appeared 19:31 UT
- ← Convection indicated from arc
- ⊙ Field-aligned current

1 **A night-side shock aurora and its three different**
2 **emissions observed on 26 February 2023**

3 **Nanjo, S.¹, M. Yamauchi², M. G. Johnsen³, Y. Yokoyama², U. Brändström²,**
4 **and K. Hosokawa¹**

5 ¹Graduate School of Communication Engineering and Informatics, The University of

6 Electro-Communications, Tokyo, Japan

7 ²Swedish Institute of Space Physics (IRF), Kiruna, Sweden

8 ³Tromsø Geophysical Observatory, Tromsø, Norway

9 **Key Points:**

- 10 • Three types of shock aurora, instead of two, are observed at 21 MLT by ground-
11 based cameras.
- 12 • They most likely correspond to three different geomagnetic signatures of an
13 SC: DL, PI, and MI.
- 14 • The propagation speeds of the current and aurora can be different for the MI
15 signature.

Corresponding author: Sota Nanjo, sota.nanjo@uec.ac.jp

16 **Abstract**

17 Ground-based observations of shock aurora, which is an aurora related to geomag-
 18 netic sudden commencement (SC), have mainly been limited to the dayside. On 26
 19 February 2023, right after the SC onset at 19:24 UT, ground-based all-sky cameras
 20 and a wide-angle camera detected shock aurora at 21 MLT in the auroral zone. For
 21 this aurora, three different emissions are detected instead of the previously known
 22 two emissions: intensification of a pre-existing arc (19:25 UT), red diffuse aurora
 23 (19:28 UT), and a second, green discrete arc (19:31 UT). The relative location of
 24 these emissions differs from the dayside cases where the first and last types are not
 25 distinguished. Geomagnetic data under this aurora indicates a significant difference
 26 in the anti-sunward propagation velocity between the secondary discrete arc and the
 27 related field-aligned current.

28 **Plain Language Summary**

29 Ground-based observations of “shock aurora” related to “sudden commence-
 30 ment (SC),” which is a sudden geomagnetic activity caused by a rapid increase of
 31 the solar wind speed (such as caused by a solar storm), were previously limited to
 32 the dayside. However, the recent development of dense networks of auroral cameras
 33 and magnetometers allows us to examine the shock aurora in the nightside from
 34 the ground. On 26 February 2023, shortly after the onset of an SC at 19:24 UT,
 35 ground-based all-sky cameras and a wide-angle camera detected the shock aurora
 36 at 21 MLT in the auroral zone. Three distinct optical emissions, instead of the two
 37 emissions previously observed on the dayside, appeared with clear time delay and lo-
 38 cational difference: intensification of a pre-existing arc (19:25 UT), red diffuse aurora
 39 (19:28 UT), and a secondary green discrete aurora (19:31 UT). There are also other
 40 differences from dayside observations: the last emission had a different propagation
 41 speed than the related field-aligned current, and the relative location of the three
 42 emissions was different.

43 **1 Introduction**

44 Geomagnetic sudden commencement (SC), which is caused by a rapid increase
 45 in solar wind dynamic pressure, consists of a stepwise increase and subsequent bipo-
 46 lar spike in the geomagnetic field (Araki, 1994, and references therein). These Dis-
 47 turbances are the most outstanding ground magnetic field perturbation at Low lat-
 48 itudes and the Polar region, hence called DL and DP, respectively. DP is normally
 49 divided into two parts, the preliminary pulse, PI, and the main pulse, MI. Following
 50 the model of Araki (1994), PI is associated with a field-aligned current (FAC) pair
 51 flowing into the afternoon auroral zone and out of the morning auroral zone while
 52 traveling anti-sunward. PI is replaced by the MI some minutes later which is a sta-
 53 tionary FAC pair of opposite directions compared to the PI pair.

54 Both disturbances are ultimately caused by an intensification of the magne-
 55 topause current, of which the information propagates globally across the geomag-
 56 netic field as the compression (this causes the DL on the ground) and as the Alfvén
 57 mode that carries FACs along the geomagnetic field, creating dusk-to-dawn and
 58 dawn-to-dusk ionospheric electric field and relevant current system (this causes the
 59 DP on the ground). Hence, the DL appears almost simultaneously (less than tens of
 60 seconds) at all magnetic local time (MLT) regions. DP (actually the PI part) also
 61 appears nearly simultaneously at all latitudes, although it is related to a current sys-
 62 tem that takes time to develop. This is because the related electric field in the iono-
 63 sphere can propagate almost instantaneously as a waveguide mode (Kikuchi, 2014).

64 Measuring the time delay from dayside to nightside is difficult because the be-
65 ginning signature of MI is hidden by the DL (and even PI). Even the peak timing
66 is not well determined because the duration and peak timing of the MI in the polar
67 cap (anti-sunward convection side) depends on latitudes (Araki & Allen, 1982). One
68 method for estimating the propagation velocity of the MI is to measure the optical
69 aurora, which is typically colocated with the intensification of FACs. The optical au-
70 rora related to an SC is actually observed by ground-based all-sky cameras (ASCs)
71 and ultraviolet (UV) imagers onboard satellites (Kozlovsky et al., 2005; Liu et al.,
72 2011), and is called shock aurora. Motoba et al. (2009) examined a shock aurora at
73 15 MLT and identified both the PI-related diffuse patch (558 nm: green) equator-
74 ward of a pre-existing arc and the MI-related discrete arc (558 nm and 630 nm: red)
75 poleward the PI-related diffuse aurora. The relative location of the MI-related arc
76 and pre-existing arc changes with the interplanetary magnetic field (IMF) and may
77 overlap with each other (seen as an enhanced oval) for the northward IMF (Nishimura
78 et al., 2016).

79 Nishimura et al. (2016) also obtained the spatial distribution of FACs and their
80 temporal development using the magnetometer network in the northern hemisphere
81 and compared it with images from ASC in Antarctica. The result suggests that the
82 PI and MI correspond to diffuse and discrete auroras in the afternoon sector, respec-
83 tively. Since the optical signature of the aurora provides a finer FAC structure than
84 what a network of geomagnetic field measurements can provide, observation by cam-
85 eras is necessary to reveal the detail of the SC current system. The method should
86 have been applied to the nightside, but the only report from the ground-based opti-
87 cal measurements is by meridian scanning photometers (Holmes et al., 2014). With-
88 out such optical observations, we do not know how the FAC develops as it propa-
89 gates to the nightside or even whether the aurora types are the same between day-
90 side and nightside.

91 According to the global imaging from satellites, the MI(PI)-related electron au-
92 rora propagates anti-sunward at about 4–6 km/s (10 km/s) on the duskside (dawn-
93 side) ionosphere (Zhou & Tsurutani, 1999; Holmes et al., 2014), and the shock au-
94 rora can extend to the midnight sector. Using multiple scanning photometers, which
95 are separately installed by about 1100 km in the evening sector and 900 km in the
96 morning sector, Holmes et al. (2014) demonstrated that the anti-sunward propa-
97 gation speed is consistent with the result from satellite observations. The derived
98 speed in the evening sector corresponds to 1–1.5 MLT/min, requiring 8 min from
99 dayside to nightside (20–22 MLT), consistent with the start of the MI signature 6
100 min after the SC onset. On the other hand, Holmes et al. (2014) detected the red
101 (630 nm) emission 1 minute before the appearance of the green (558 nm) aurora,
102 which indicates that low-energy electrons may have precipitated into the ionosphere
103 3 min prior to the high-energy (> 1 keV) electrons if we take into account the av-
104 erage relaxation time of the red aurora of about 2 min. The FAC corresponding to
105 the duskside red aurora must have arrived much earlier than the source FAC for the
106 green aurora in Holmes et al. (2014), giving a quite different anti-sunward propaga-
107 tion speed between the source of the red aurora and that of the green aurora.

108 To summarize our understanding so far, there are two types of shock aurora in
109 addition to pre-existing arc: the PI-related and MI-related auroras, and they might
110 have different propagation speeds from each other. If so, the difference in the ap-
111 pearance time of these auroras would be larger on the nightside than on the day-
112 side. In addition, the relative location of these auroras and even the fine structure
113 might also be different between dayside and nightside. To clearly distinguish these
114 auroras and their temporal development on the nightside, we need observations of
115 multi-wavelength cameras and a dense meridional network of the magnetometer in
116 the auroral region.

117 On 26 February 2023, right after an SC onset at 19:24 UT, a color ASC in
 118 Kiruna that was located at 21 MLT (65° geomagnetic latitude) detected (1) the en-
 119 hancement of a pre-existing green arc (19:25 UT), (2) the appearance of a red diffuse
 120 aurora (19:28 UT), and (3) a secondary green arc (19:31 UT) at unexpected location
 121 (equatorward of the pre-existing arc), with the geomagnetic MI peak at 19:27 UT.
 122 We also observed the secondary arc with a high-time resolution wide-angle camera,
 123 which revealed the vortex motion of the arc. The shock aurora was weakened within
 124 20 min, and this interval was isolated from the subsequent substorm growth phase.
 125 The shock aurora appeared above the densely distributed magnetometer network
 126 (IMAGE), and the relative location of FACs and aurora can be derived in good reso-
 127 lution. Here we report these combined observations of the shock aurora seen 3 hours
 128 before the magnetic midnight.

129 2 Instruments

130 2.1 All-sky cameras (ASCs)

131 We analyzed all-sky images from cameras in Kiruna, Sweden (67.83°N , 20.42°E)
 132 and Skibotn, Norway (69.35°N , 20.36°E). In Kiruna, a Sony $\alpha 7\text{S}$ with a Nikkor 8mm
 133 F2.8 lens was installed. The camera's ISO was set at 4000, and the exposure time
 134 was 10–13 sec. Images were taken every minute. At Skibotn Observatory, a Sony
 135 $\alpha 6400$ with a MEIKE MK-6.5mm F2.0 lens was in operation. The camera's ISO was
 136 set at 8000, and the exposure time was 8 sec. Images were taken every 30 sec. We
 137 used these images to geolocate and identify spatiotemporal variations of the aurora.

138 2.2 Wide-angle camera (WAC)

139 A Sony $\alpha 7\text{SIII}$ with an FE 24mm F1.4 GM lens was installed at a dome where
 140 the Kiruna ASC was located. This camera, called wide-angle camera (WAC), faces
 141 in the north-northeast direction at a low elevation with an angle of view of ~ 73 de-
 142 grees horizontally, covering an area marked by a white rectangle in the last panel of
 143 Figure 2. WAC recorded videos at 30 frames per second, offering a high temporal
 144 resolution for visualizing auroral movement within 1 minute. WAC has 1920×1080
 145 pixels, an ISO sensitivity of 80000, and a 1/30 second exposure time. We averaged
 146 15 images (for 0.5 seconds) to make snapshots to reduce noise, as shown in Figure 3.
 147 We provide a video of the event as Supporting Information.

148 2.3 Magnetometers

149 A selection of magnetometers from the IMAGE network has been applied in
 150 the study. These are stable flux-gate magnetometers, providing 10-second resolution
 151 data. Furthermore, the low latitude, Intermagnet magnetometer at Huancayo has
 152 been used.

153 3 Observation Results

154 Figures 1a and 1b shows the IMF (intensity in black and the z component in
 155 red) and solar wind dynamic pressure, respectively, from the Deep Space Climate
 156 Observatory (DSCOVR). A stepwise enhancement of the IMF intensity and dynamic
 157 pressure, a typical signature of the interplanetary shock, was detected at around
 158 18:40 UT. Figure 1c shows the H component of the geomagnetic field recorded by
 159 magnetometers located in Sørøya (SOR), Norway (70.54°N , 22.22°E); Tromsø (TRO),
 160 Norway (69.66°N , 18.94°E); Kilpisjärvi (KIL), Finland (69.02°N , 20.79°E); Kiruna
 161 (KIR), Sweden (67.83°N , 20.42°E); and Huancayo (HUA), Peru (12.06°S , 75.21°W).
 162 Their locations, except HUA, are shown in Figure 1g. HUA is instead located on the

163 dayside equator at ~ 14.2 MLT, which is the typical SC onset region. All the sta-
 164 tions show the SC signature starting at around 19:24 UT. This SC is isolated from
 165 the substorm activity that started around 20:20 UT, and hence we show only the
 166 short time interval in Figure 1e (19:21–19:32 UT). The onset time ($\sim 19:24:00$ UT)
 167 is marked by a dashed line (left). Similarly, the peak time of the PI ($\sim 19:25:20$ UT)
 168 is also marked by another dashed line (right).

169 Figures 1d and 1f show the keogram, the time series of the north-south cross-
 170 section of the all-sky images from Kiruna ASC. Note that the exposure time changed
 171 from 10 to 13 sec at 19:28 UT. The keogram shows that the aurora appeared shortly
 172 (~ 15 min) after the SC, and its intensity gradually increased for the first ~ 10 min.
 173 Figure 1f shows a time lag between the magnetic signatures and the auroral intensi-
 174 fication.

175 In Figure 1g, all-sky images obtained by the ASCs in Kiruna and Skibotn at
 176 19:33 UT are projected on the map showing the locations of the magnetic stations
 177 and cameras. Coordinates with an elevation angle of more than 20 degrees were
 178 used for the projection, and the auroral emission layer was assumed to be 100 km.
 179 The projected aurora is found close to the zenith of Kilpisjärvi and Tromsø (67.5°
 180 MLAT, 21 MLT).

181 Figure 2 is a minute-by-minute all-sky image from 19:23 to 19:34 UT. The up-
 182 per side of each image is north, and the left side is east. The solid white line in the
 183 first panel shows the cross-section used to make keograms shown in Figure 1. The
 184 first all-sky image at 19:23 UT, taken before the SC onset, already shows a weak
 185 diffuse aurora (circled by the white dashed line) in the northeast direction. In this
 186 paper, we refer to this aurora as the pre-existing arc. The third all-sky image was
 187 taken 1 minute after the onset and shows that the arc is stronger than before the on-
 188 set, as indicated by the yellow arrow. At 19:28 UT, as indicated by the red arrow,
 189 a red emission became visible south of the pre-existing arc that was further intensi-
 190 fied. This intensification causes the automatic change in the exposure time from 13
 191 to 10 sec. At 19:31 UT, discrete arcs with wavy structures were detected between
 192 the pre-existing arc and the red emission at both the west (right) and east (left)
 193 sides. They were connected at 19:32 UT and formed an arc from west to east, and
 194 the wavy structure became stronger afterward. In this paper, we refer to this arc
 195 as the secondary arc. The last four all-sky images (19:31–19:34 UT) show the quick
 196 evolution of the secondary arc every minute. The 1-min resolution is apparently too
 197 low to visualize the exact fine spatiotemporal evolution of the secondary arc. For-
 198 tunately, we have a 30 Hz video taken by WAC. WAC captured the white rectangle
 199 region in the last all-sky image in Figure 2.

200 Figure 3 shows the images taken by WAC observing the area shown in the last
 201 panel of Figure 2. The images obtained from 19:34.12.1 to 19:35:08.1 UT are shown
 202 every 8 seconds. In the electronic version of this paper, a real-time video of this se-
 203 quence is provided as Supporting Information. Note that the east-west direction of
 204 the image is reversed from the all-sky image. The meridian with an azimuth angle of
 205 0 degrees (northward) is shown as a dotted line in panel (a). In each snapshot, two
 206 auroral structures are visible with a spatial gap near the center of the image. Both
 207 wavy structures gradually steepened by the westward motion on the front side (low
 208 latitude side) and eastward motion on the back side (high latitude side), as indicated
 209 by the white arrows. As this steepening developed, these structures consequently
 210 formed a spiral shape.

4 Discussion

The shock aurora was observed by ASCs and the high-speed WAC in the evening sector at around 21 MLT. Three components of shock aurora were identified instead of only two (PI-related diffuse aurora and MI-related arc), which was the case for the dayside afternoon sector. Their characteristics are summarized in Figure 4, in which the locations of the aurora are illustrated in the polar view.

1. Pre-existing weak arc (green, most likely 558 nm) was gradually intensified right after the SC onset at 19:24 UT.
2. Red diffuse aurora (apparently 630 nm) gradually appeared widely in the longitudinal direction equatorward of the intensified pre-existing arc, as shown in Figure 4a. This aurora became visible at 19:28 UT, i.e., 4 min after the onset.
3. Discrete green (secondary) arcs suddenly appeared between the red diffuse aurora and the intensified pre-existing arc at two separated spots (west and east in the WAC images). They became visible at 19:31 UT (7 min after the SC onset) and developed before start moving.

We also examined a video from the EMCCD ASC in Tjautjas, Sweden (attached as Supplemental Information), and found that the western and eastern arcs seen at 19:31 UT in Figure 2 appeared at around 19:30:52 and 19:31:12 UT, respectively. Both arcs did not propagate gradually but appeared as jump as independent clumps. The jumping speed from west to east (about 0.5 MLT apart) is about 1.5 MLT/min. After the appearance, both arcs started expanding in the east-west direction (Figure 4b) and got connected to each other. Subsequently, they showed the vortex motion without changing their locations, as shown in Figure 4c. The secondary arc might be accompanied by the red emission (most likely 630 nm) at high latitudes, but it is difficult to examine the continuity from the ASC images.

Considering the average relaxation time of ~ 2 min for the red diffuse aurora, the precipitation of the low-energy electrons might have started only 1–2 min after the SC onset. In the evening sector, diffuse auroras are generally associated with downward FAC, whereas intensified arcs are generally associated with upward FAC (e.g., Marklund et al., 2011). Therefore, the pre-existing arc (upward FAC) and red diffuse aurora (downward FAC) may be related to the DL and PI, respectively. In other words, the DL might also have generated the shock aurora by intensifying the pre-existing arc for the present case. If so, the past dayside observation of the MI-related aurora might be contaminated by the DL-related aurora.

The time delay of the appearance of the secondary arc from the SC onset was 7 min (and 5–6 min from the MI onset); thus, the anti-sunward propagation speed from the noon sector is about 1.5 MLT/min. This value is similar to the propagation/expansion speed of the MI-related arc in the afternoon sector (Motoba et al., 2009; Holmes et al., 2014; Nishimura et al., 2016). The nightside propagation speed estimated by the jumping of the secondary arc was also similar, about 1.5 MLT/min. Such an agreement indicates that the propagation of the MI-related aurora may be in the form of a leap rather than a continuous extension.

The secondary arc was located equatorward of the intensified pre-existing arc and overlapped with the red diffuse aurora, indicating that the source electric field existed at an L-shell in the middle of the ring current region. This implies that the affected areas in the nightside magnetosphere by the DL, PI, and MI are not in the same latitudinal order as the dayside signature in terms of the L-shell. This is not impossible if we consider the difference in the propagation velocities of the DL (compression) and DP (Alfvénic). If the relative latitude of the aurora is reversed between dayside and nightside, we must interpret the result from the meridian scan-

261 ning photometer (e.g., Holmes et al., 2014) in a different manner between dayside
 262 and nightside.

263 The present result also provides new insight into the anti-sunward propaga-
 264 tion speed of the FAC structure. Since the approximate FAC intensity is calculated
 265 from the latitudinal gradients of the H component of the geomagnetic field from
 266 the ground, the peak of FAC intensity read from Figure 1e (SOR, TRO, KIL, and
 267 KIR) is at 19:27 UT, i.e., 3 min after the SC onset at 19:24 UT. If we consider the
 268 start time of this gradient, the FAC already intensified at 19:26 UT, only 2 min after
 269 the SC onset. This means that the FAC propagated from dayside to 21 MLT with
 270 a speed of at least 4 MLT/min. This is much faster than the propagation speed of
 271 the MI-related aurora (1.5 MLT/min). Then the question is why the time delay be-
 272 tween the FAC and aurora intensification increases as it propagates anti-sunward.
 273 This question remains for future investigation.

274 Figures 3 and 4c show that the auroral vortex develops nearly stationary, sug-
 275 gesting that the anti-sunward convection poleward of the arc and sunward convec-
 276 tion equatorward of the arc have similar speeds. Such stationarity raises a ques-
 277 tion on the convection: how does the convection develop as the SC signature and
 278 shock aurora propagate anti-sunward? Together with the leap-like appearance, the
 279 formation of the aurora and its relation to the current system needs future investi-
 280 gations. Fortunately, modern optical instruments are rapidly improving their sen-
 281 sitivity, and the number of optical stations is increasing. Furthermore, the incom-
 282 ing SMILE (Solar wind Magnetosphere Ionosphere Link Explorer) mission to be
 283 launched in 2024–2025 would give a long-time global UV monitor from almost the
 284 same location. Combining its image with improved ground-based optical ability will
 285 allow systematic studies of the shock aurora on the nightside.

286 5 Conclusion

287 We observed the nightside shock aurora with ground-based all-sky cameras and
 288 a high-speed wide-angle camera at 21 MLT. Unlike the dayside shock aurora, where
 289 only two types of (PI- and MI-related) emissions are reported, we identified three
 290 emissions: enhancement of the pre-existing arc, the red diffuse aurora, and the dis-
 291 crete arc. These emissions most likely correspond to three different geomagnetic sig-
 292 natures of an SC: DL, PI, and MI. We believe that this is the first time observation
 293 of DL-related emission. For the MI signature, the anti-sunward propagation speed of
 294 the field-aligned current seems to be much faster than that of the related aurora. In
 295 addition, the relative location of the MI-related aurora and intensified pre-existing
 296 arc is not necessarily the same between the dayside and nightside.

Open Research Section

The all-sky images from Kiruna are available at <https://www.irf.se/alis/allsky/krn/2023/02/26/19/>. The all-sky images from Skibotn are available at http://darndeb08.cei.uec.ac.jp/~nanjo/public/skibotn_imgs/2022_season/20230226/. The solar wind data from DSCOVR are available at <https://www.ngdc.noaa.gov/dscovr/portal/index.html#/>. The magnetometer data from Huancayo is provided through INTERMAGNET <https://www.intermagnet.org>. Other magnetometer data are available at <https://flux.phys.uit.no/stackplot/>.

Acknowledgments

We thank Huancayo Geomagnetic Observatory and Finnish Meteorological Institute that provided the magnetometer data from Huancayo and Kilpisjärvi, respectively. We thank T. Araki for his valuable advice on SC. This work was partly supported by Grants-in-Aid for Scientific Research (15H05747, 22H00173, 21J20254) from the Japan Society for the Promotion of Science (JSPS). The first author of this study is a research fellow DC of JSPS.

References

- Araki, T. (1994). A physical model of the geomagnetic sudden commencement. In *Solar wind sources of magnetospheric ultra - low - frequency waves* (p. 183-200). American Geophysical Union (AGU). Retrieved from <https://agupubs.onlinelibrary.wiley.com/doi/abs/10.1029/GM081p0183> doi: <https://doi.org/10.1029/GM081p0183>
- Araki, T., & Allen, J. H. (1982). Latitudinal reversal of polarization of the geomagnetic sudden commencement. *Journal of Geophysical Research: Space Physics*, *87*(A7), 5207-5216. Retrieved from <https://agupubs.onlinelibrary.wiley.com/doi/abs/10.1029/JA087iA07p05207> doi: <https://doi.org/10.1029/JA087iA07p05207>
- Holmes, J. M., Johnsen, M. G., Deehr, C. S., Zhou, X.-Y., & Lorentzen, D. A. (2014). Circumpolar ground-based optical measurements of proton and electron shock aurora. *Journal of Geophysical Research: Space Physics*, *119*(5), 3895-3914. Retrieved from <https://agupubs.onlinelibrary.wiley.com/doi/abs/10.1002/2013JA019574> doi: <https://doi.org/10.1002/2013JA019574>
- Kikuchi, T. (2014). Transmission line model for the near-instantaneous transmission of the ionospheric electric field and currents to the equator. *Journal of Geophysical Research: Space Physics*, *119*(2), 1131-1156. Retrieved from <https://agupubs.onlinelibrary.wiley.com/doi/abs/10.1002/2013JA019515> doi: <https://doi.org/10.1002/2013JA019515>
- Kozlovsky, A., Safargaleev, V., Østgaard, N., Turunen, T., Koustov, A., Jussila, J., & Roldugin, A. (2005). On the motion of dayside auroras caused by a solar wind pressure pulse. *Annales Geophysicae*, *23*(2), 509-521. Retrieved from <https://angeo.copernicus.org/articles/23/509/2005/> doi: 10.5194/angeo-23-509-2005
- Liu, J. J., Hu, H. Q., Han, D. S., Araki, T., Hu, Z. J., Zhang, Q. H., . . . Ebihara, Y. (2011). Decrease of auroral intensity associated with reversal of plasma convection in response to an interplanetary shock as observed over zhongshan station in antarctica. *Journal of Geophysical Research: Space Physics*, *116*(A3). Retrieved from <https://agupubs.onlinelibrary.wiley.com/doi/abs/10.1029/2010JA016156> doi: <https://doi.org/10.1029/2010JA016156>
- Marklund, G. T., Sadeghi, S., Cumnock, J. A., Karlsson, T., Lindqvist, P.-A., Nilsson, H., . . . Zhang, Y. (2011). Evolution in space and time of the quasi-static acceleration potential of inverted-v aurora and its interaction with alfvénic

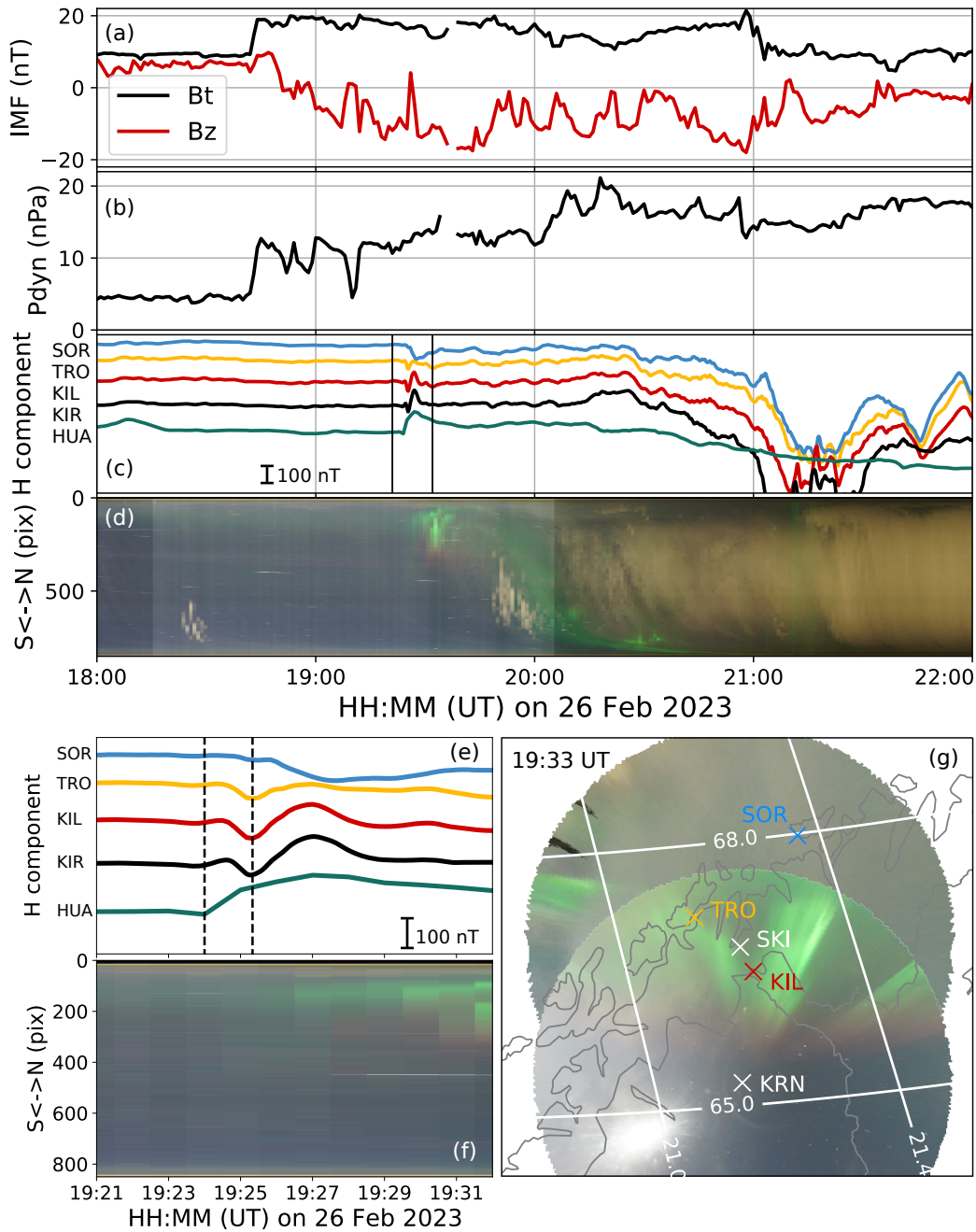


Figure 1. (a–b) The intensity (black) and z component (red) of the interplanetary magnetic field and solar wind dynamic pressure from DSCOVR. (c) Magnetometer data from the stations in the auroral and equatorial regions. A scale of 100 nT is shown in the lower left. (d) North-to-south keogram from the Kiruna ASC. (e–f) Close-up views of panels (c) and (d) from 19:21 to 19:32 UT. Vertical dashed lines indicate the onset of the SC and peak time of the PI. (g) Projection of all-sky images from the Kiruna and Skibotn ASCs. The location of the magnetometers is also shown. The grid line gives the magnetic local time and latitude.

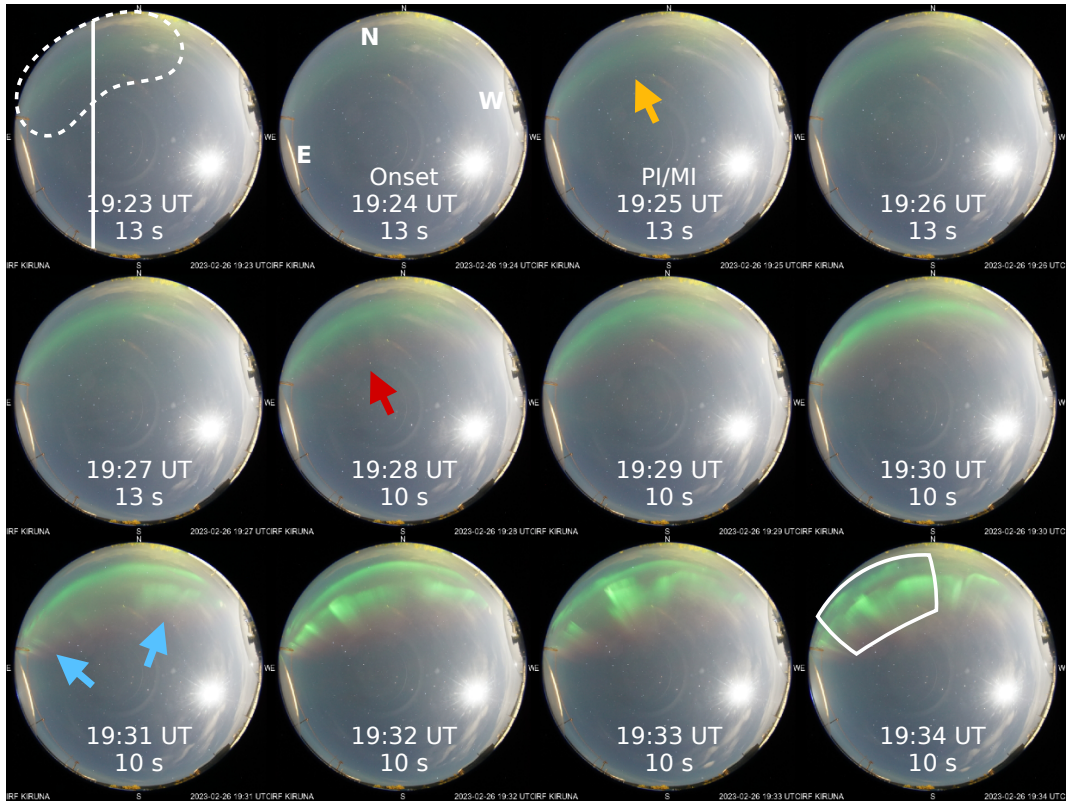


Figure 2. The ASC images from Kiruna during 19:23–19:34 UT on 26 February 2023. The top is north, and the left is east. The white dashed region in the first panel shows the pre-existing arc. The appearance of the red aurora and secondary arc is marked by red and blue arrows, respectively. The white rectangle region in the last panel is the FoV of the images shown in Figure 3.

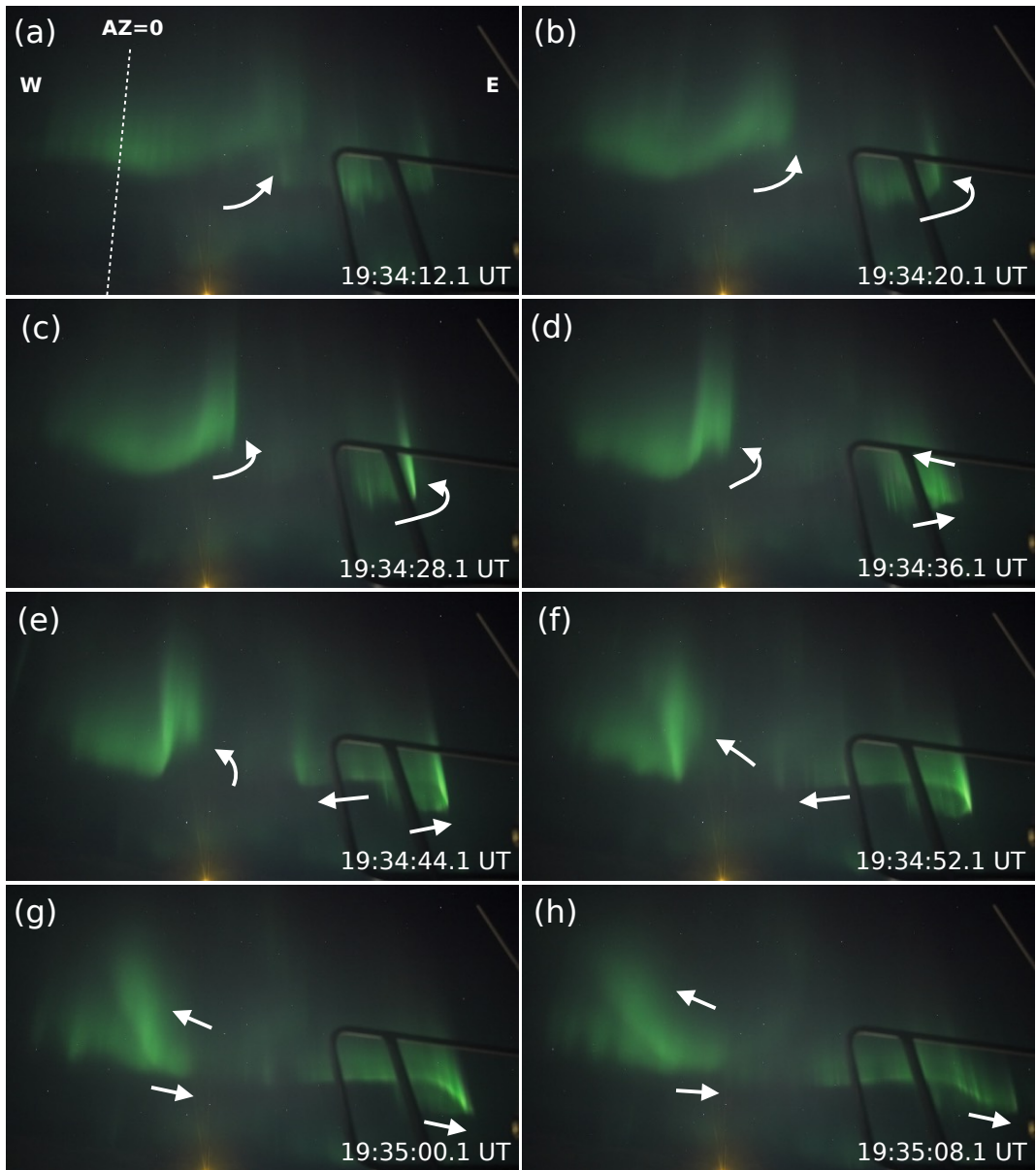


Figure 3. The wide-angle images captured by the Sony $\alpha 7SIII$ camera during 19:34:12–19:35:08 UT. The right side is east (different from the ASC image). The white dashed line in the first panel indicates the meridian, which has an azimuth angle of 0 degrees (towards the north). The white arrows guide the vortex motion.

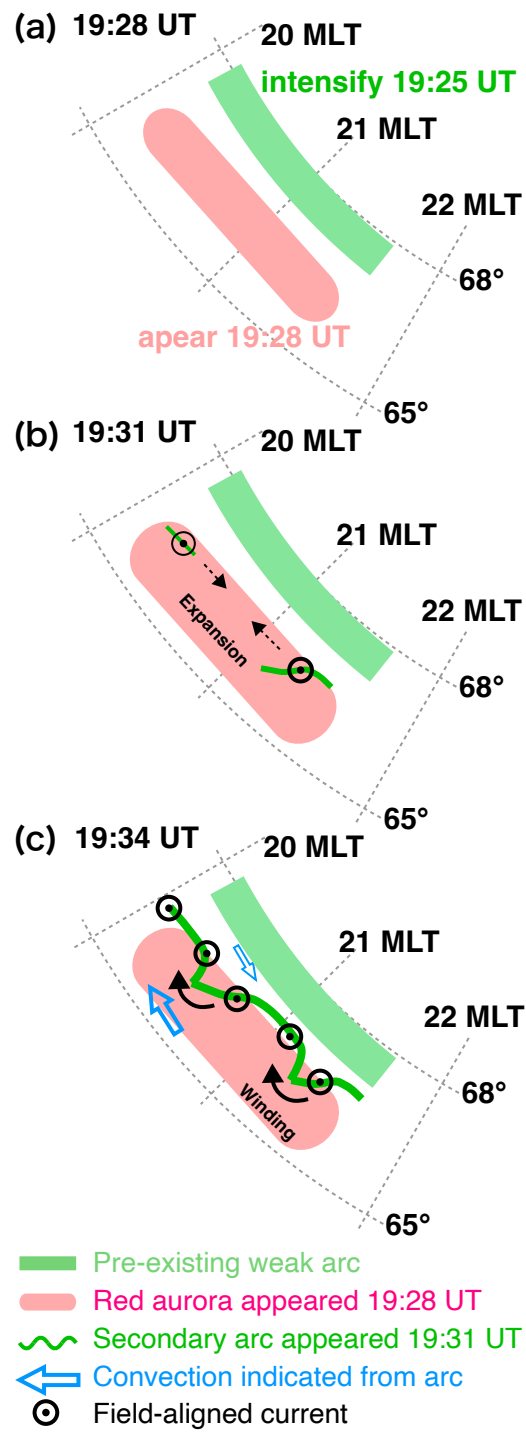


Figure 4. Schematic illustration of the relative locations of pre-existing arc, red diffuse aurora, and secondary arc. The blue arrows indicate the convection directions suggested by the vortex motion of the secondary arc.

- 348 boundary processes. *Journal of Geophysical Research: Space Physics*, 116(A1).
349 Retrieved from [https://agupubs.onlinelibrary.wiley.com/doi/abs/](https://agupubs.onlinelibrary.wiley.com/doi/abs/10.1029/2011JA016537)
350 [10.1029/2011JA016537](https://doi.org/10.1029/2011JA016537) doi: <https://doi.org/10.1029/2011JA016537>
- 351 Motoba, T., Kadokura, A., Ebihara, Y., Frey, H. U., Weatherwax, A. T., & Sato,
352 N. (2009). Simultaneous ground-satellite optical observations of postnoon
353 shock aurora in the southern hemisphere. *Journal of Geophysical Research:*
354 *Space Physics*, 114(A7). Retrieved from [https://agupubs.onlinelibrary](https://agupubs.onlinelibrary.wiley.com/doi/abs/10.1029/2008JA014007)
355 [.wiley.com/doi/abs/10.1029/2008JA014007](https://doi.org/10.1029/2008JA014007) doi: [https://doi.org/10.1029/](https://doi.org/10.1029/2008JA014007)
356 [2008JA014007](https://doi.org/10.1029/2008JA014007)
- 357 Nishimura, Y., Kikuchi, T., Ebihara, Y., Yoshikawa, A., Imajo, S., Li, W., & Utada,
358 H. (2016, Aug 11). Evolution of the current system during solar wind pressure
359 pulses based on aurora and magnetometer observations. *Earth, Planets and*
360 *Space*, 68(1), 144. Retrieved from [https://doi.org/10.1186/s40623-016](https://doi.org/10.1186/s40623-016-0517-y)
361 [-0517-y](https://doi.org/10.1186/s40623-016-0517-y) doi: [10.1186/s40623-016-0517-y](https://doi.org/10.1186/s40623-016-0517-y)
- 362 Zhou, X., & Tsurutani, B. T. (1999). Rapid intensification and propagation of
363 the dayside aurora: Large scale interplanetary pressure pulses (fast shocks).
364 *Geophysical Research Letters*, 26(8), 1097-1100. Retrieved from [https://](https://agupubs.onlinelibrary.wiley.com/doi/abs/10.1029/1999GL900173)
365 [agupubs.onlinelibrary.wiley.com/doi/abs/10.1029/1999GL900173](https://doi.org/10.1029/1999GL900173) doi:
366 <https://doi.org/10.1029/1999GL900173>